Oxidation processes in the Eastern Mediterranean atmosphere: Evidence from the Modelling of HOx Measurements over Cyprus

Chinmay Mallik[1], Laura Tomsche[1], Efstratios Bourtsoukidis[1], John N. Crowley[1], Bettina Derstroff[1], Horst Fischer[1], Sascha Hafermann[1], Imke Hueser[1], Umar Javed[1], Stephan Kessel[1], Jos Lelieveld[1,2], Monica Martinez[1], Hannah Meusel[3], Anna Novelli[4], Gavin J. Phillips[5], Andrea Pozzer[1], Andreas Reiffs[1], Rolf Sander[1], Domenico Taraborrelli[4], Carina Sauvage[1], Jan Schuladen[1], Hang Su[2], Jonathan Williams[1,2] and Hartwig Harder[1]

[1] Atmospheric Chemistry Dept., Max Planck Institute for Chemistry, Mainz, 55128, Germany
[2] Energy, Environment and Water Research Center, Cyprus Institute, Nicosia, 1645, Cyprus
[3] Multiphase Chemistry Dept., Max Planck Institute for Chemistry, Mainz, 55128, Germany
[4] Institute of Energy and Climate Research, Forschungszentrum Juelich GmbH, Julich, 52425, Germany
[5] Department of Natural Sciences, University of Chester, Chester, CH1 4BJ, United Kingdom

Correspondence to: Hartwig Harder (hartwig.harder@mpic.de) & Chinmay Mallik (chinmay.mallik@mpic.de)

Abstract. The Mediterranean is a climatically sensitive region located at the crossroads of air masses from three continents: Europe, Africa and Asia. The chemical processing of air masses over this region has implications not only for the air quality, but also for the long-range transport of air pollution. To obtain a comprehensive understanding of oxidation processes over the Mediterranean, atmospheric concentrations of the hydroxyl radical (OH) and the hydroperoxyl radical (HO_2) were measured during an intensive field campaign (CYprus PHotochemistry EXperiment, CYPHEX-2014) in the north-west of Cyprus in the summer of 2014. Very low local anthropogenic and biogenic emissions around the measurement location provided a vantage point to study the contrasts in atmospheric oxidation pathways under highly processed marine air masses and those influenced by relatively fresh emissions from mainland Europe.

The CYPHEX measurements were used to evaluate OH and HO_2 simulations using a photochemical box model (CAABA/MECCA) constrained with CYPHEX observations of O_3, CO, NO_x, hydrocarbons, peroxides and other major HO_x (OH + HO_2) sources and sinks in a low NO_x environment (<100 pptv NO). The model simulations for OH showed very good agreement with in-situ OH observations. Model simulations for HO_2 also agreed fairly well with in-situ observations except when pinene levels exceeded 80 pptv. Different schemes to improve the agreement between observed and modelled HO_2, including changing the rate coefficients for the reactions of terpene generated peroxy radicals (RO_2) with NO and HO_2 as well as the autoxidation of terpene generated RO_2 species, are explored in this work. The main source of OH in Cyprus was its primary production from O_3 photolysis during the day and HONO photolysis during early morning. Recycling contributed about one-third of the total OH production, and the maximum recycling efficiency was about 70 %. CO, which was the largest OH sink was also the largest HO_2 source. Lowest HO_x production and losses occurred when the air masses had higher residence time over the oceans.

1. 1 Introduction

1.1. Air pollution and HO_x chemistry

The chemical and photochemical processing of air pollutants, in conjunction with local emissions, meteorology and atmospheric transport, strongly influences the air quality over a region. The regional air quality impacts human health,
5 agriculture, the overall condition of the biosphere and subsequently the climate. Studies attribute 2-4 million premature deaths globally to outdoor air pollution (Silva et al., 2013; Lelieveld et al., 2015). Oxidants in the Earth's atmosphere prevent the pollutants released into it from building up to toxic levels. These oxidants not only convert many toxic pollutants into less toxic forms (e.g. CO to CO_2) but also help in their removal (e.g. NO_x and SO_2 are converted into soluble HNO_3 and H_2SO_4 respectively), although some toxic chemicals may still be formed during degradation of non-toxic ones. Most of the
10 oxidation processes in the atmosphere proceed along reaction pathways initiated by the hydroxyl radicals (OH) during the day (Levy, 1971), making it the dominant chemical cleaning agent of the daytime atmosphere (Lelieveld et al., 2004). The dominant primary production of OH is via the photolysis of O_3 at ultraviolet wavelengths (Crosley, 1995) producing the electronically excited $O(^1D)$ atoms (R1). O^1D that escapes quenching (R2) reacts with water vapor in the atmosphere to produce OH radicals (R3)

15   $O_3 + h\nu \rightarrow O(^1D) + O_2$ (R1, λ<330 nm)

  $O(^1D) + M \rightarrow O(^3P) + M(M = N_2, O_2)$ (R2)

  $O(^1D) + H_2O \rightarrow 2OH$ (R3)
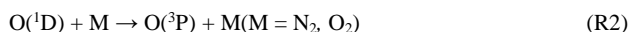
Because of its fast reactions (e.g. R4) with several biogenically and anthropogenically emitted gases, the lifetime of OH in the troposphere is typically a few hundred milliseconds. Oxidation limits these gases (CH_4, CO, volatile organic compounds)
20 from accumulating above trace levels in the troposphere. Reactions of OH with CO and hydrocarbons (R4) also trigger quasi-instant formation of the hydroperoxyl radical (HO_2, via R5) in our O_2 rich atmosphere. In the presence of NO and O_3 (R6, R7), a chemical equilibrium is set between OH and HO_2 on a timescale of seconds. The sum of OH and HO_2 is known as HO_x. The reactions R6 and R7 maintain the oxidizing efficiency of the atmosphere by recycling OH. Simultaneously, in the presence of NO_x (=NO + NO_2), they also propel a reaction chain leading to O_3 formation via R8 and R9. R8-R9 are the
25 main chemical source of tropospheric O_3, which is an important oxidant, a greenhouse gas as well as a major secondary pollutant.

  $CO + OH \rightarrow CO_2 + H$ (R4)

  $H + O_2 (+M) \rightarrow HO_2 (+M)$ (R5)

  $NO + HO_2 \rightarrow NO_2 + OH$ (R6)

30   $HO_2 + O_3 \rightarrow OH + 2O_2$ (R7)

$$NO_2 + h\nu \rightarrow O(^3P) + NO \qquad\qquad (R8, \lambda < 430\ nm)$$

$$O(^3P) + O_2\ (+M) \rightarrow O_3\ (+M) \qquad\qquad (R9)$$

OH also oxidizes anthropogenic and biogenic hydrocarbons (HCs) emitted into the atmosphere leading to peroxy radicals (RO$_2$). NO converts the RO$_2$ into HO$_2$, which again leads to OH recycling (R6). The HO$_x$ cycle can be terminated by the

5 radical+radical interactions of RO$_2$ and HO$_2$ with and between themselves to form peroxides (R10, R11). Depending on NO levels, the RO$_2$ species can react through different channels. Under low NO$_x$ conditions e.g. in clean marine boundary layer, when the reaction of RO$_2$ with NO is less significant than its reaction with HO$_2$, peroxide formation becomes a major sink for HO$_2$, further leading to OH and O$_3$ removal. Under higher NO levels, RO$_2$ would react with NO to form NO$_2$ (O$_3$ source), HO$_2$ (OH source), alkyl nitrates as well as aldehydes (R12, R13, R14). Further, there have been suggestions of auto-

10 oxidation of RO$_2$ to produce peroxides and yielding OH under atmospheric conditions (Crounse et al., 2013). These auto-oxidation mechanisms proceed through catalytic H-shifts at a very fast rate (upto ~ 0.1s^{-1}) e.g., conversion of RO$_2$ generated from a carbonyl compound into a highly functionalized dicarbonyl hydroperoxide compound (R15).

$$HO_2 + HO_2 \rightarrow H_2O_2 + O_2 \qquad\qquad (R10)$$

$$RO_2 + HO_2 \rightarrow ROOH + O_2 \qquad\qquad (R11)$$

15 $$RO_2 + NO + O_2 \rightarrow R'CHO + HO_2 + NO_2 \qquad\qquad (R12)$$

$$RO_2 + NO \rightarrow RNO_3 \qquad\qquad (R13)$$

$$NO_2 + OH + M \rightarrow HNO_3 + M\ (M = N_2, O_2) \qquad\qquad (R14)$$

H$_3$C—C(=O)—CH(O-O·)—CH$_3$	+ O$_2$	→	H$_3$C—C(=O)—C(=O)—CH(O-OH)—CH$_3$	+ OH (R15)
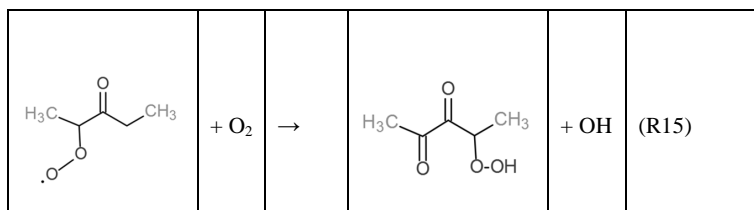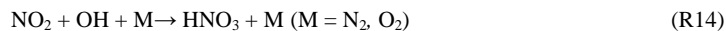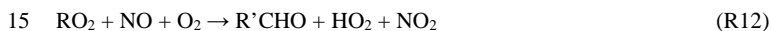
In polluted air when NO$_x$ concentrations become large enough that the reaction of NO$_2$ with OH dominates over other HO$_x$ sinks, the major loss of HO$_x$ is via the formation of nitric acid (HNO$_3$, R14), which is then removed from the atmosphere by

20 wet and dry deposition. Some acid forming reactions are also the starting point of particle formation in the atmosphere e.g. via oxidation of SO$_2$. In sum, oxidation is a means by which major pollutants are processed and removed from the atmosphere, but with concomitant implications to air quality, agriculture, climate and health. However, large uncertainties in atmospheric reaction pathways, rate coefficients and measurements of atmospheric gases and radicals, limit our ability to understand and predict the quality of ambient air.

1.2. Motivation for the campaign

The Mediterranean is a climatically sensitive region which is rapidly getting warmer and dryer over time (Lelieveld et al., 2012). The atmospheric chemistry over the region is complex with regular exceedances of the European Union (EU) ozone air quality standard (Doche et al., 2014; Kalabokas et al., 2013) and a projected increase of summertime O_3 over the Eastern
5 Mediterranean (Lelieveld et al., 2002; Lelieveld and Dentener, 2000). Cyprus is a small, remote island (area: 9251 km²; population: 1.15 x 10⁶; Density: 119.2 people/km²) in the Eastern Mediterranean (south of mainland Europe) with very low local emissions. The non-methane volatile organic compounds (NMVOCs), NO_x, SO_x emitted by Cyprus and European Union (EU28) were 6.8, 17.2, 16.8 Gg and 6722, 7819, 3083 Gg respectively for 2014 (European Union emission inventory report, 2017). Being located downwind of the mainland Europe emissions, Cyprus provides an ideal vantage point to study
10 the impact of European emissions on the Mediterranean climate (Lelieveld et al., 2002). To study the atmospheric chemistry over the Mediterranean and understand the impact of emissions from different regions of Europe on air quality in Cyprus, an intensive field measurement campaign (the Cyprus Photochemistry EXperiment, hereafter CYPHEX) was conducted in Cyprus during the summer of 2014, wherein a comprehensive suite of trace gases was measured.

Cyprus is exposed to air masses influenced by emissions from South-West European countries which are photo-chemically
15 processed over the Mediterranean Sea. The Etesian winds during summer carry air masses loaded with emissions from industry and biomass burning over Central/East European countries. Although emissions from Europe have been steadily decreasing over the past few decades (e.g. NO_x, SO_x and NMVOCs decreased by nearly 50 %, 80 % and 57 % respectively during 1990-2013; European Union emission inventory report, 2017), these emissions are still substantial having significant global impact. Apart from the influence of European emissions, Cyprus is strategically located at cross-roads of air masses
20 from Asia, Africa and the Atlantic (Kleanthous et al., 2014). Influence from all these different source regions, incorporating the impact of a plethora of hydrocarbons, nitrogen and sulfur species as well as mineral dust on the atmospheric processing in this part of the world, have attracted several field campaigns (Carslaw et al., 2001; Berresheim et al., 2003). For example, the Mediterranean INtensive Oxidant Study (MINOS) was conducted to study the budget of atmospheric oxidants influenced by long-range transport of pollution, in the summer of 2001 (Lelieveld et al., 2002; Gros et al., 2003; Salisbury et al., 2003).
25 OH radicals were measured in the coastal boundary layer of Crete as part of the MINOS campaign and the major sources of OH were found to be photolysis of O_3 and recycling from HO_2+NO reaction (Berresheim et al., 2003). Although HO_2 was not measured during MINOS, high levels of HCHO, a major primary HO_2 source, were observed (Kormann et al., 2003). In the present study, we report simultaneous measurements of OH and HO_2 during the CYPHEX campaign, and compare these observations with simulations from a photochemical box model constrained with O_3, CO, NO, NO_2, peroxides, several
30 anthropogenic and biogenic hydrocarbons including important alkanes, alkenes, alkynes, aldehydes and acids and photolysis frequencies of important gases relevant to HO_x chemistry. The main objective of this study is to identify the major chemical species and reaction pathways controlling the HO_x chemistry over this climatically sensitive region.

2. Methods

2.1 Measurement site

35 The CYPHEX campaign was conducted at the northwest coast of Cyprus, on a hilltop about 650 m AMSL, in Paphos District of the island and facing the sea about 5-8 km away on the west. The Akamas peninsula national park is about 25 km to the northwest of the measurement site (34° 57' N / 32° 23' E), with terrain descending rapidly to the northeast towards the town of Polis, with a population of about 2000. The area comprises of spare shrub type vegetation with small Mediterranean trees comprising pines, junipers, olives, carob, pomegranates, and almonds. The area is weakly populated in a radius of about
40 20 km. The site is away from the major cities: Paphos with 90000 people is 20 km south, Limassol with 235000 people is 70

km south east, Larnaca with 145000 people is 110 km east and Nicosia with 325000 people is 90 km north-east (census of population Oct 2011; www.cystat.gov.cy). The local wind direction is predominantly south-west (70 % between 202.5° - 247.5°) (Meusel et al., 2016; Derstroff et al., 2017), bringing in humid air from the sea, with no immediate anthropogenic influence. Analysis of 5 day back trajectories show mainly two major air mass regimes (Huser et al., 2017). Etesian winds
5   influenced by fresh emissions from East-Central Europe and crossing Turkey and Greece, and Mistral winds influenced by emissions from south-west Europe but processed for a longer period over the Mediterranean (Figure 1). During the summer of 2014, a weakened east-west pressure gradient led to weak and delayed Etesian winds (Tyrlis et al., 2015). The site is also influenced by local land sea breezes.

2.2 HO$_x$ measurements during CYPHEX

10   Atmospheric OH and HO$_2$ were measured during CYPHEX using the HydrOxyl Radical measurement Unit based on fluorescence Spectroscopy (HORUS) instrument (Martinez et al., 2010). The setup was based on the well-established Laser Induced Fluorescence-Fluorescence Assay by Gas Expansion (LIF-FAGE) technique for atmospheric OH measurements (Brune et al., 1995; Crosley, 1995; Hard et al., 1984). The laser system consisted of a tunable dye laser which was pumped by a diode-pumped Nd:YAG laser (Navigator I J40-X30SC-532Q, Spectra Physics) pulsing at 3 kHz. The two laser
15   assemblies were mounted on either side of a vertical plate, which was mounted on a rack inside a measurement container about 6 m x 2.5 m x 2.5 m. The output laser radiation was split in a 9:1 ratio using beam splitters, and channeled through 8 m optical fibers into the detection module for measurements of OH and HO$_2$.

The detection system was mounted about 6 m above ground level (AGL) on the top of a scaffolding tower, constructed close to the wall of an air-conditioned container adjacent to the Laser unit. The container with the HORUS instrument was
20   mounted on top of another similar measurement container with O$_3$, CO, NO$_x$ and peroxide instruments inside. The inlets for all the instruments measuring during CYPHEX were placed within 5 m of the HORUS detection unit on the tower. Ambient air was drawn in HORUS through a critical orifice with pinhole size of 0.9 mm into a detection cell with about 4.3 mbar pressure. This internal pressure was achieved by using a combination of a roots blower (M90 compressor from Eaton, USA) followed by a scroll pump (XDS 35i, Edwards, USA). The resulting high volume flow ensured that the exchange of air
25   illuminated by the laser is fast enough between two consecutive pulses, thus avoiding possible laser-induced interferences.

The interaction of the ambient air with the laser beam in the low pressure detection cell was maximized using a White cell setup, where the laser light was reflected 32 times across the detection volume. The OH molecules were selectively excited by 308 nm laser light pulsing at 3 kHz on resonance with the Q$_1$(2) transition line (A$^2\sum$–X$^2\prod$, v'=0 ←v''=0). An etalon controlled by a stepper motor, in the dye laser setup, caused the laser radiation to be tuned on and off resonance with the OH
30   transition every 7 s to account for the OH fluorescence plus background signals and the background signals, respectively, resulting in a time resolution of 14 s. The spectra from a reference cell, where OH was produced by H$_2$O thermolysis, was used to detect the Q$_1$(2) line. The counts from the reference cell were used to sustain the on-resonance position while the etalon tethered around it. Although the pressure reduction in the detection cell results in smaller numbers of OH molecules, it improves the OH fluorescence quantum yield due to reduced collisional quenching of excited OH radicals. The lifetime of
35   the excited OH extends beyond the Mie scattering by aerosols and the Raleigh scattering by smaller molecules/particles. These interfering background signals were discriminated by using time-gated micro-channel plate detectors (Hamamatsu), enabling excitation of OH radicals and detection of fluorescence at the same wavelength. The excitation at 308 nm is advantageous to the excitation at 282 nm as interference from laser generated OH from O$_3$ photolysis is ~25 times smaller at 308 nm. A band pass filter with a central wavelength of 308 ± 0.75 nm and bandwidth of 5 nm (FWHM) in front of the
40   detector prevented signals due to any interfering wavelengths from registering on the detector. The fluorescence decay was recorded with a time-resolution of 4 ns and integrated for on-resonance and off-resonance periods, thus delineating the signal

from the spectroscopic background. Further, the spectra of the measured atmospheric OH was compared with the one obtained from a reference cell ensuring no interferences from fluorescence of species like SO_2 and naphthalene.

The chemical background, originating from OH being internally produced during the transit time of about 3 ms from the orifice to the center of the detection cell, was accounted for by removing ambient OH with an OH scavenger. This

5 scavenger, 3-5 sccm of pure propane in a carrier flow of 8000 sccm synthetic air for CYPHEX, was introduced through an inlet pre-injector (IPI) mounted on top of the inlet nozzle (Novelli et al., 2014a; Hens et al., 2014). The scavenger amount was just sufficient to scavenge off ~95% of atmospheric OH as determined from propane titration experiments on-site. IPI was connected to a blower that draws about 180-200 lpm of ambient air from the top of the IPI, the flow being monitored by a differential pressure sensor. The OH scavenger was injected via eight 0.5 mm diameter holes 5 cm above the pinhole of the

10 OH inlet into the center of the air flow sampled by IPI close to its hyperbolic minima (Novelli et al., 2014b). The hyperbolic internal shape of the IPI (max cross section of 35 mm and min cross section of 6 mm) helps to sample air that has minimum wall contact and flows at a high velocity through a small diameter ensuring that the scavenger is well mixed with atmospheric air. The high flow also ensures minimum impact of the horizontal wind speed on the mixing efficiency. The IPI cycling was automated by a script resulting in repeated cycles of scavenger injection, flushing and no injection. The

15 scavenger was periodically injected every 2 min, resulting in alternating measurements of background OH and total OH i.e. with and without scavenger injection. The difference between these two signals gives a measure of the atmospheric OH with a time resolution of 4 min. The wall losses in the IPI were periodically determined by physically dismounting the IPI for 5 min during measurements during different times of the day. On average, the background signal was 45 % of the total signal during daytime (Supplementary Figure 1). While the constituents of background OH can have pronounced impact on

20 atmospheric oxidation processes, especially over regions with high biogenic emissions (Mauldin et al., 2012), the study of the influence of background OH on oxidation pathways during CYPHEX is beyond the scope of the present study.

Atmospheric HO_2 was measured in a detection cell located 16 cm below the OH detection block. HO_2 measurements were achieved by injecting NO purified through a sodium hydroxide coated silica (Sigma-Aldrich Ascarite) using a 1/8'' od, 0.035'' id coiled stainless steel loop with about 3 cm diameter, placed just above the HO_2 detection block. The NO was

25 injected through 0.1 mm holes, leading to conversion of HO_2 into OH and detected by the same principle as in the first block. To minimize impact of RO_2 on OH formation (Fuchs et al., 2011; Hens et al., 2014), only about 30 % of atmospheric HO_2 was converted to OH using NO. The required NO flow, about 0.5 sccm pure NO in 10 sccm carrier flow during CYPHEX, was determined from titrations in ambient and calibration air. Tests were done with and without NO to ensure that there was no influence of HO_2 conversion into OH in the first axis. The measurement in the HO_2 detection cell yields the total HO_x

30 (OH + HO_2). HO_2 is calculated as the difference between HO_x and the OH measured in the first axis, after accounting for the relative OH sensitivities of the two detection axes.

Calibration of the instrument for OH and HO_2 measurements is achieved by measuring the signals generated by known amounts of OH and HO_2 (Martinez et al., 2010) in a calibrator setup. The calibrator was mounted on top of the OH inlet without the IPI. Known amounts of OH and HO_2 were produced by irradiating different concentrations of humidified air

35 with 185 nm radiation produced by a pen ray Hg lamp. The actinic flux density of the Hg lamp (Pen-ray line source, LOT-Oriel, Germany) used for the photolytic radical production was determined before and after the campaign using the actinometry method by N_2O photolysis (Martinez et al., 2010). Different H_2O mixing ratios were produced by mixing different combinations of humidified and dry air flows using mass flow controllers. The humidified air was generated by bubbling dry air into a container half-filled with water and heated at about 80°C. The water mixing ratio in the humid air

40 stream was measured by a LICOR CO_2/H_2O-Analyzer (Li-7000) based on the detection of differential absorption with an IR spectrometer. The stability of the Li-7000 was ensured by calibrations with a dew point generator (Li-610 from LICOR).

The precision and minimum detection limit for OH measurements during CYPHEX was determined from the variability of the background signals (Table 1). The chemical background, during propane injection, being larger than the spectroscopic background (off-resonance), has a dominating impact on the precision. The precision for OH and HO_2 measurements were calculated to be $4.8e^5$ molecules cm^{-3} and 0.39 pptv, respectively for 4 min and 14 sec time resolutions, respectively. The

5 accuracy for OH measurements was derived from the uncertainties in OH calibrations, which involve uncertainties in determination of lamp flux (traceable to a NIST NO standard), flows (calibrated with a DC-2B, traceable to IS0/RVA 17025), H_2O mixing ratios (calibrated with a Li-610) and uncertainties in estimation of OH losses in the IPI, accumulating to 28.5% (2σ). The accuracy in HO_2 measurements was estimated to be 36 % (2σ) based on calibrations, loss of HO_2 in the IPI and the uncertainty in NO mixing during titrations.

10 **2.3 Measurements of other Chemical and Meteorological parameters**

During CYPHEX, measurement instruments (Table 1) were set-up in four air-conditioned laboratory containers, placed in two stacks of two. An 8 m tall, 0.5 m diameter, high flow ($10 m^3 min^{-1}$) common inlet installed between the stacks was used to draw ambient air for most instruments. The references to the various measurements are indicated in Table 1. C_2-C_4 alkanes and alkenes (ethane: C_2H_6, ethene: C_2H_4, propane: C_3H_8, propene: C_3H_6, butane: C_4H_{10} (i and n), butene: C_4H_8 (c and t) were

15 measured with a time resolution of 60 min and the mixing ratio represents an average over a sampling period of 20 min (Sobanski et al., 2016). Photolysis frequencies were obtained by a CCD Spectroradiometer (Metcon GmbH) operating at 275-640 nm with a 2-π integrating hemispheric quart dome. The spectroradiometer was calibrated prior to the campaign using a 1000 W NIST traceable irradiance standard. Photolysis frequencies were calculated using molecular parameters recommended by the IUPAC and NASA evaluation panels (Sander et al., 2011; IUPAC, 2015). An automatic weather

20 station (Vantage Pro2; Davis Instruments Corp., Hayward, CA) was used to measure temperature, pressure, wind direction and speed, solar radiation and humidity with a time resolution of 1 min.

2.4 The CAABA/MECCA model

Due to the high reactivity of OH with a plethora of anthropogenic and biogenic hydrocarbons, the HO_x chemistry of the atmosphere involves numerous reactions. To efficiently evaluate these reactions, several mechanisms of various complexity

25 have been developed, e.g. the Regional Atmospheric Chemical Mechanism (RACM; (Stockwell et al., 1997), the Master Chemical Mechanism (MCM; http://mcm.leeds.ac.uk), the Mainz Isoprene Mechanism (MIM; (Taraborrelli et al., 2009), the Carbon Bond Mechanism (Yarwood and Rao, 2005), etc. For this study, we use the Module Efficiently Calculating the Chemistry of the Atmosphere (MECCA, Sander et al., 2011; Sander et al., 2005) , which is an atmospheric chemistry module that contains a comprehensive set of gas and aqueous phase chemical reaction mechanisms covering tropospheric

30 and stratospheric chemistry. The gas phase chemistry in the present version contains 2664 species (including 40 dummy species to account for deposition) and 1670 reactions, including basic O_3, CH_4, HO_x, NO_x, NMHC and sulfur chemistry. Complex organic chemistry is taken from the Mainz Organic Mechanism (MOM, Taraborrelli et al., 2015). MOM is based upon the MIM3, containing new additions to an isoprene oxidation mechanism (MIM2) for regional and global atmospheric modelling. Under pristine conditions, isoprene oxidation buffers OH to a narrow range of concentrations (Taraborrelli et al.,

35 2009). The original MIM is based on the MCM. MIM2 was further developed to improve the tropospheric chemistry under a wide range of NO_x regimes, and provided a better evaluation of NO_x and organic nitrogen-containing species due to a detailed representation of the alkyl and peroxy acyl nitrates as well as isoprene oxidation products, some of which can be measured by modern instrumentation e.g. MVK, methacrolein (MACR), hydroxyacetone and methyl glyoxal (Taraborrelli et al., 2009). MIM3 is a reduced version of MIM2, suitable for 3D atmospheric chemistry-transport modelling. It contains an

40 improved isoprene oxidation mechanism related to OH recycling. It accounts for the photo-oxidation of unsaturated hydroperoxy-aldehydes, a product of isoprene oxidation; initiating a hydroxyl radical production cascade. Compared to RACM, MIM3 presents a lower degree of lumping and reproduces the mixing ratios of the main chemical species in the

atmosphere and many intermediates very well under a tropical mid-NO$_x$ scenario (Taraborrelli et al., 2012). In MIM3, the extended chemistry following the OH and O$_3$ pathways has been thoroughly revised, tested in a box model, and shown to reproduce HO$_x$ measurements, even for challenging conditions with high isoprene mixing ratios (>1 nmol mol^{-1}) and low NO (< 40 pmol mol^{-1})(Taraborrelli et al., 2012). For the numerical integration, MECCA uses the KPP software (Sandu and
5 Sander, 2006). All gas-phase reactions are contained in a single chemical file (gas.eqn).

The most common method to efficiently evaluate a complex chemical environment is to use a zero dimensional, photochemical box model. Here, we use version 3.8 of the box model CAABA (Chemistry As A Boxmodel Application) which is based on version 3.0 described by (Sander et al., 2011). To apply the MECCA chemistry to atmospheric conditions, it is connected to the CAABA base model via the MESSy interface. The model is constrained by observed concentrations of
10 the main reactive trace gases, O$_3$, CO, NO, NO$_2$, HONO, HCHO, H$_2$O$_2$, MHP, SO$_2$, C$_2$-C$_4$ alkanes and alkenes, isoprene, pinene (α and β), limonene, benzene, toluene, methane, methanol, acetonitrile, acetaldehyde, acetone, acetic acid, as well as photolysis rate constants. Model results were obtained by letting the model run into steady state for OH and HO$_2$ for each set of data points. The steady state was set to be achieved for OH when the relative changes in OH was less than 5 x 10^{-7}. Deposition velocities used in our scheme for some important species are provided in Table 2. The deposition is incorporated
15 into the model scheme by converting a species into a dummy species according to its deposition velocity. As these dummy species will not participate in any further chemical reaction, their precursors are effectively removed from the model chemical scheme. The deposition velocities of peroxides, formic and nitric acid are based on (Nguyen et al., 2015) while those for PINAL and PAN are based on (Evans et al., 2000) using the average of the deposition rates for water, forest and grass. The model scheme is included in the supplementary of this manuscript.

20 **2.5 The FlexPart model**

In order to understand the impact of different emission sources on the atmospheric processing of air masses, the dynamical transport history of air parcels reaching Cyprus during the CYPHEX campaign was traced using FlexPart 9.2 (Stohl et al., 2005). FlexPart is a Lagrangian particle dispersion model that describes the transport and diffusion of tracers by computing the trajectories of large number (ca. 10000) of infinitesimally small tracer particles. For CYPHEX, trajectory simulations
25 were done at 3-hour time intervals during 21-31 July 2014. For this, FlexPart was run 120 hours backward in time from the measurement site driven with analyses from the ECMWF with 0.2° x 0.2° horizontal resolution and a temporal resolution of 1 hour (Huser et al., 2017). The particle density distribution of the tracer particles during this 120 hour backward simulation provided information on their residence time in each grid cell of the defined geographical area (Supplementary Figure 2). Major transport routes of air reaching the site during CYPHEX were identified from the grid cells with higher residence
30 times.

3. Results and discussion

3.1 HO$_x$ measurements during CYPHEX and associated meteorological and chemical parameters

The variation of OH and HO$_2$ along with a few important chemical and radiation parameters relevant to HO$_x$ chemistry during 21 July-1 August (Day of the year: 202-213) is shown in Figure 2. The mean values of OH and HO$_2$ during 21 July-1
35 August were 2.2 x10^6 and 2.87x10^8 molecules per cm^3 respectively. The mean OH concentration during peak noon hours (J(O^{1}D)>2e^{-5} s^{-1}) was 5.75x10^6 molecules per cm^3. While both OH and HO$_2$ showed a clear diurnal variation, the HO$_2$-OH ratio decreased with enhancement in J(O^{1}D), and was close to 100 at J(O^{1}D)=3e^{-5} s^{-1}. During the MINOS campaign in the summer of 2001 in Crete, an island in the Central Mediterranean at similar latitude about 700 km west of the CYPHEX site,

average OH levels were measured to be 3.6-6.7 x 10^6 molecules per cm^3 (Berresheim et al., 2003). The peak OH levels during MINOS reached twice the peak values observed during our study in Cyprus. During MINOS, OH peaked at about 2.1 x 10^7 molecules per cm^3, with O_3 and $J(O^1D)$ of about 60 ppbv and $2.8e^{-5}$ s^{-1}. These O_3 and $J(O^1D)$ values are not very different from CYPHEX values, indicating that the peak primary OH production would not be very different for MINOS and
5   Cyprus. Although HO_2 was not measured during MINOS, the CO levels (mean values reaching close to 160 ppbv) were much higher (Heland et al., 2003) compared to CYPHEX indicating possibility of higher HO_2. Nevertheless, the absence of HO_2 measurements during MINOS impairs our ability to directly compare the OH chemistry from the two datasets for a regional perspective. However, the peak OH levels observed during CYPHEX are comparable to the midday OH concentrations predicted for the Finokalia Aerosol Measurement Experiments (FAME-08) at a remote coastal site on the
10   island of Crete, Greece (Hildebrandt et al., 2010). The FAME measurements showed the presence of aged, highly oxygenated organic aerosols (OA) during summer compared to winter despite being heavily influenced by continental air masses (53 %) during summer and aged marine air masses (61 %) during winter. The presence of highly oxygenated OA during summer were attributed to strong photochemical impacts due to higher O_3 and UV and levels during summer, leading to double the values of midday OH concentrations during summer compared to winter (Hildebrandt et al., 2010).

15   While OH measurements during CYPHEX started on 12 July, 2014 (day number: 193), systematic HO_2 measurements started much later from 21 July, 2014 (day number: 202). Simultaneous measurements of OH and HO_2 during CYPHEX are available for the period 21-31 July, and the discussion in this work is based on this common dataset. Large day to day changes in concentrations of several OH and HO_2 precursors were observed during the study period e.g. O_3 varied from 50-110 ppbv, CO from 70-140 ppbv, HCHO from 0.2-2 ppbv. The noontime OH and HO_2 levels were $5.75x10^6$ ($\pm$43%) and
20   $6.25x10^8$ ($\pm$30%) molecules per cm^{-3} respectively (Fig. 2). While the average concentrations of O_3 and CO during the study period (Day Number: 202-212) were 69 and 104 ppbv respectively, during the days 205, 206, the mean O_3 and CO values were 22 and 33 % lower. The later period i.e. days 205 and 206 correspond to air masses arriving from South-Western Europe and passing over the Mediterranean with predominantly marine influence (reaching over 70 % for 5 day simulations using FlexPart). The large changes in O_3 and CO under different air mass regimes do not translate into the changes in HO_x
25   levels (Figure 2). This is because their concentrations are to some extent buffered as sources and sinks tend to increase in parallel in relation to anthropogenic/biogenic emissions. To study the impact of these numerous reactions on the HO_x budget, we used a photochemical box model (CAABA/MECCA).

3.2 Modelling simulations of CYPHEX HO_x

Figure 3 shows simulations of OH and HO_2 using CAABA/MECCA in comparison with the measurements in ambient air.
30   Due to remote location of the measurement site, it is expected that the HO_x chemistry would be representative for the background Mediterranean atmosphere. In general, NO levels were low during CYPHEX, with only ~2 % of data above 1 ppbv NO and ~5 % above 100 pptv NO. The study is limited to NO below 100 pptv to exclude measurements affected by emissions from the local diesel generator and local automobile traffic. Under very remote conditions, the steady state of HO_x would be achieved from a balance between HO_x production (R1-R3) and HO_x loss (R10). However, such a simplified
35   condition is rarely achieved in the boundary layer as the presence of hydrocarbons leads to additional production and loss channels. A first model run was done constraining only O_3, CO, CH_4, NO, NO_2, HONO, HCHO and H_2O_2, H_2O and photolysis frequencies to measured values (Figure 4 case I). Thus, the major primary production channels for OH and HO_2 via photolysis of O_3, HONO and HCHO are constrained by measured quantities, while the recycling of OH and HO_2 occurs via reactions with O_3, CO, CH_4 and NO only. However, in the absence of the contribution from important hydrocarbons, OH
40   loss is underestimated leading to an over-prediction of OH in the order of 88 %. Further, HO_2 is also overestimated, on average, by more than 30 % in this case (Figure 4 case I) as loss via formation of hydroperoxides is under represented due to the incomplete VOC representation leading to too low RO_2 concentrations.

When we constrain the model with all measured species, the OH simulations are much improved with a model to measured ratio of 0.90 (Figure 3 case III). However, HO_2 is now underpredicted by about 17 %. The underprediction of HO_2 is enhanced with increasing terpene (α-pinene, β-pinene and limonene) mixing ratios, with average HO_2 model/measurement ratio of 0.72 for >80 pptv of measured terpenes. When terpenes are not included in the model, the HO_2 simulations are much

5   improved (model/measured=1.02). The mean daytime OH reactivity of the measured major terpenes was about 0.06 s^{-1}. This value is only 3.7 % of the calculated reactivity from the total of all measured species and about 10.7% of the OH reactivity (k_{OH}; Eq. 1) from CO. The OH reactivity calculated from the trace gases measured during CYPHEX varied between 1-2 s^{-1} during the study period (Figure 4), which is comparable to reactivity measurements made in the free troposphere (Mao et al., 2009). During the TORCH-2 campaign in Weybourne, England and the DOMINO campaign in El Arenosillo, Spain, the

10   total reactivity was generally <5 s^{-1} when air masses originated from the sea (Lee et al., 2009; Sinha et al., 2012). The OH reactivity measured in sub-urban regions is generally higher than 5 s^{-1} (Yang et al., 2016). During CYPHEX, CO and CH_4 constituted more than half of the total calculated reactivity (Figure 4). CO, CH_4, HCHO, C_5H_8 and CH_3CHO accounted for 35, 17, 13, 9 and 8 % respectively of the calculated OH reactivity for daytime values during CYPHEX.

$$k_{OH}= \sum (k_{species} \text{ x } C_{species}) \qquad\qquad\qquad (Eq 1)$$

15   where $k_{species}$ is the rate coefficient for reaction of a given species with OH and $C_{species}$ is the concentration of the same species.

As limonene chemistry is not included in the current model scheme, it is accounted for in the model in form of additional α-pinene after normalizing for their OH reactivities. When limonene is included as CH_4 instead of α-pinene, the OH loss increases by about 1 % compared to case II when there were no terpenes in the model, which confirms the average OH

20   reactivity of limonene at 0.02 s^{-1} i.e. an additional 1 % of the calculated reactivity from the measured species. Although limonene chemistry is different from α-pinene in that it caters more towards secondary organic aerosols (SOA) formation, addition of limonene as α-pinene increases HO_2 and OH losses by 3-6 %, which is well within the uncertainty of the measurements. Nevertheless, the degradation products from terpene oxidation (shown in Figure 5) further act as sources and sinks for OH and HO_2, hence play an important role in the overall HO_x chemistry (Calogirou et al., 1999; Librando and

25   Tringali, 2005; Zhang et al., 2015; Wisthaler et al., 2001). Further, increasing/decreasing the terpene concentrations by their measured uncertainties (15 %; Table 1) decreases/increases the OH and HO_2 model/measured slope by 2-3 %, which is close to the errors on the regression slopes. Also, changing other gases like CO and C_5H_8 by their uncertainties (Table 1) has less than 3 % impact on the model vs measured slopes for OH and HO_2. Nevertheless, when terpenes are included as CH_4, both OH are HO_2 simulations are much improved (Figure 3 case IV). In this case, the terpene chemistry does not play any role in

30   OH-HO_2 simulations but the primary OH reactivity of terpenes is taken into account.

Review studies show agreements between in-situ observations of OH and HO_2 and box model calculations using different chemical schemes within a factor of 2 for both for urban and marine (boundary layer) environments (Stone et al., 2012). During the North Atlantic Marine Boundary Layer Experiment (NAMBLEX) field campaign in the summer of 2002 at the Mace Head Atmospheric Research Station, OH was underpredicted early in the morning and in the late afternoon/early

35   evening and overpredicted in the middle of the day based on simple steady state calculations (Smith et al., 2006). However, photolysis of HONO was not considered due to the absence of HONO measurements during NAMBLEX. The authors contemplate that HONO photolysis and OH recycling could play crucial roles in explaining the discrepancy between measured and calculated OH during periods with high solar zenith angle. Despite low isoprene regimes (Lewis et al., 2005), inclusion of DMS and C_5H_8 improved calculated/measured ratio for OH from 1.13±0.36 to 0.94±0.39 during NAMBLEX.

40   HO_2 was overpredicted but model performance improved by incorporating reactions with BrO, IO and aerosol uptake; the best case scenario for HO_2 modeled/measured was 1.26±0.36. During the Intercontinental Chemical Transport Experiment-A (INTEX-A) , OH was predicted fairly well for the lowest 2 km over North America and the western Atlantic Ocean using a

zero-dimensional, time-dependent photochemical box model developed at NASA Langley Research Center (Ren et al., 2008). In the study, HO_2 was overpredicted (model/measurement=1.37). It is challenging to put the model-measurement agreement during CYPHEX in perspective of other studies, because they vary with respect to chemical regimes i.e. different amount of NO_x and hydrocarbons as well as the chemical mechanisms employed to simulate the HO_x chemistry. (Rohrer et
5 al., 2014) compared the HO_x chemistry from different field campaigns using a common modelling framework, and point to buffering mechanisms that maintains OH in various NO_x and VOC regimes. (Ren et al., 2008) have noted that despite highly constrained measurement suites during various field campaigns, there are significant discrepancies between model predictions and actual measurements of OH and HO_2 in different environments. One possible reason for the discrepancy could be due to unmeasured atmospheric constituents. However, during CYPHEX we have been able to measure the major
10 primary sources and sinks related to HO_x chemistry and simulations agree within uncertainty of OH and HO_2 measurements. Another plausible reason for discrepancy is the uncertainty in mechanistic pathways, branching ratios and rate constants etc., which are not known with sufficient accuracy. A recent study comparing 7 different chemical mechanisms constrained with the same input data and boundary conditions revealed 25-40 % ambiguity in predictions of HO_2 and OH over the United States (Knote et al., 2015). As we highlight in the next section, also the HO_x chemistry related to terpenes is associated with
15 substantial uncertainty.

3.3 Reasons for decreased model accuracy when including the terpene chemistry
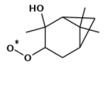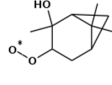
As discussed in the last section, we find that the underprediction in HO_2 gradually increases with increasing terpene levels, being about 38 % for the highest terpene levels observed (about 120 pptv). To ascertain if this underprediction is related to terpene chemistry or some other chemical pathway, we compare two model runs viz. case III vs case IV in Figure 3. Case IV
20 is achieved by initializing the model with zero terpenes, however keeping the terpene reactivity towards OH intact. The terpene reactivity i.e. the product of individual terpene concentrations with their rate coefficient towards OH is approximated in the model scheme in form of additional CH_4 (Figure 3, case IV). Under this scenario, we find that the agreement between modelled and observed HO_2 again improves, to levels similar to case II without terpenes in the model (Figure 3). The small difference of 6 % with respect to OH prediction between these cases II and IV (Figure 3) also corroborates the minor
25 primary reactivity of <0.06 s^{-1} for the sum of α-pinene, β-pinene and limonene towards OH. However, up to 38 % underprediction in HO_2 for terpene concentrations over 80 pptv indicates the important role of secondary products formed during terpene oxidation towards the HO_x budget.
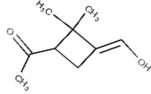
To quantify the magnitude of the impact of terpene degradation products in the HO_x budget, we compared the HO_x sinks from the two model cases: case III (Figure 3, henceforth 'terpene case') and case II (Figure 3, henceforth 'isoprene case'),
30 the difference being the presence and absence of α-pinene, β-pinene and limonene. The estimation of HO_x sinks from the two model cases is conspicuously marked by significant contribution of terpene degradation/oxidation products in the terpene case which are absent in the isoprene case. The additional reactions in the terpene case make up 6.3-27.8 % of the total HO_x sinks, the contributions increasing with the terpene concentrations and peaking between 13-14 hours Local Time on clear days (Figure 5). While the terpene degradation products contribute, on average, 15 % to the total HO_x loss, this value is 20.5
35 % for terpenes>80 pptv. The corresponding contribution of terpene related peroxy radicals to the total HO_x loss is 7.8 and 10.3 % respectively, accounting for about 52 % of the impact of the terpene degradation products, including peroxy radicals, pinal, norpinal and peroxides, towards HO_x loss.

Since only about 3.7 % of primary terpene reactivity with OH results in up to 28 % of HO_x loss, with terpene generated peroxy radicals having more than four times the impact of the primary terpenes to the HO_x loss, we examine a sequence of
40 reactions starting with the oxidation of α-pinene to understand the genesis and propagation of these terpene generated peroxy radicals (R15-R23). The reactions show that oxidation of α-pinene via OH and O_3 directly generates several peroxy radicals (R15-R16) which are a sink for HO_x via their reactions with HO_2 forming hydroperoxides (e.g. R21-R22). These first

generation peroxy radicals also form other peroxy radicals (R17-R20), and the chain propagates to produce additional peroxy radicals contributing via formation of the respective hydro peroxide in reaction with HO_2 leading to overall HO_x loss (e.g. R23).

+ OH	→ 0.75	$C_{10}H_{17}O_3$ (APINABO2)	+0.15	HO_2	+…	(R15, G40200 in Model)
+ O_3	→ .09	$C_{10}H_{17}O_3$ (APINABO2)	+ .33	$C_9H_{14}O_2$ (Norpinal)	+ .77 OH + .33 CO + .33 HO_2 +….	(R16, G40232 in Model)
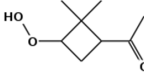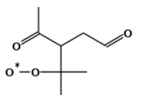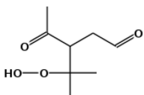
$C_9H_{14}O_2$ (Norpinal)	+ hv	→	$C_9H_{14}O_2$ (Norpinenol)	(R17, J49203b in Model)
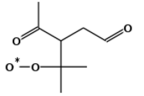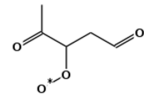
C$_9$H$_{14}$O$_2$ (Norpinal)	+ hv	→	C$_8$H$_{13}$O$_3$ (C85O2)	+ CO + HO$_2$	(R18, J49203a in Model)
C$_9$H$_{14}$O$_2$ (Norpinal)	+ HCOOH	→	C$_9$H$_{14}$O$_2$ (Norpinenol)	+ HCOOH	(R19, G49248 in Model)

C$_9$H$_{14}$O$_2$ (Norpinenol)	+ OH	→	C$_8$H$_{13}$O$_4$ (C86O2)	+ HCOOH + OH	(R20, G49246 in Model)

 C₈H₁₃O₃ (C85O2)	+	HO₂	→	 C₈H₁₄O₃ (C85OOH)	(R21, G48201 in Model)
 C₈H₁₃O₄ (C86O2)	+	HO₂	→	 C₈H₁₄O₄ (C86OOH)	(R22, G48206 in Model)

 C₈H₁₃O₄ (C86O2)	→	 C₅H₇O₄ (C511O2)	+ CH₃COCH₃	(R23, G48204 in Model)

Thus, a cascade of HO_x scavengers mostly in the form of RO_2 species, at low NO_x levels, starting with oxidation of primary terpenes leads to nearly 28 % HO_x loss, resulting in up to 38 % underprediction of HO_2. The losses increase with increases in terpene levels. The major contribution towards the HO_x loss comes from terpene generated organic peroxy radicals (Figure 3). However, there are major uncertainties regarding the chemical pathways and rate coefficients governing the chemistry of these peroxy radicals in the actual atmosphere and in the next section we examine several postulates based on the literature.

3.4 Terpene generated organic peroxy radicals

A limitation in our understanding of peroxy radical oxidation pathways is the rate constant of peroxy radicals with NO. For most peroxy radicals, lumped rate coefficients are defined by the expression Eq. 2 (Rickard and Pascoe, 2009) as kinetic data are unavailable for most of the RO_2-NO reactions.

$$K_{RO2NO} = 2.54 \times 10^{-12} \exp(360/T).f \qquad \text{Eq 2}$$

Thus, K_{RO2NO} is the product of the rate coefficient and an efficiency factor, f. The values of f for different classes of RO_2 are given in (Jenkin et al., 1997). The reaction of RO_2 with NO can proceed via two channels, one forming alkyl nitrate ($RONO_2$) and the other forming RO and NO_2 (R12-R13). Enhancing the RO_2-NO rate coefficient suppresses the peroxide forming channel via HO_2. For our study period, increasing the $KRO2NO$ even by a factor of 4 led to only a 6.8 % increase in modelled HO_2 levels for terpenes> 80 pptv (Figure 6).

During the summertime 1999 Southern Oxidant Study (SOS99) at Nashville, Tennessee, agreement could be found between photochemical models and in-situ measurements when the product of the branching ratio and rate constant for organic peroxide formation, via R11, was reduced by a factor of 3-12 (Thornton et al., 2002). To test this hypothesis, we decreased the K_{RO2HO2} for terpenes by half and by one-fifth of its value considered in the model. The rate coefficient of RO_2 with HO_2 leading to ROOH is given by Eq. (3), where K_{RO2HO2} increases with the size of RO_2 radicals (Atkinson et al., 1999; Boyd et al., 1996) http:// mcm.leeds.ac.uk/MCMv3.3.1/categories/ saunders-2003-4_6_4-gen-master.htt?rxnId=6942).

$$K_{RO2HO2} = 2.91 \times 10^{-13} \exp(1300/T) [1 - \exp(-0.245n)] \qquad \text{Eq 3}$$

where n is the carbon number and T is the temperature.

We find that decreasing the rate coefficient of by a factor of 5 leads to better reconciliation with our observations than when decreasing it by a factor of 2. When K_{RO2HO2} was reduced by a factor of 5, the modelled HO_2 increased by only 9.9 % for higher terpene levels i.e. α-pinene+ β-pinene+limonene>80 pptv (Figure 6).

Recent studies have proposed inter and intramolecular hydrogen abstraction by peroxy radicals (autoxidation) to be effective reaction pathways leading to OH formation (Crounse et al., 2013). This abstraction is largely determined by the thermochemistry of the nascent alkyl radicals and thus is strongly influenced by neighboring substituents, hence the rate

increases rapidly when more oxygen containing functional groups are involved. The H-shift rates reported in literature can be as fast as 0.1 s^{-1} for atmospheric conditions. We incorporated a simple autoxidation scheme for some of the most important terpene related RO$_2$ species as specified in figure 5 in our model. In this scheme, the specific terpene generated RO$_2$ species whose contribution was at least 0.25 % to the HO$_x$ sink are converted into a corresponding ROOH at a very fast

5 rate (1e^{10} x K$_{RO2HO2}$) reaching up to 0.2 s^{-1},e.g. C$_{10}$H$_{15}$O$_4$ (PINALO2) is converted to C$_{10}$H$_{16}$O$_4$ (PINALOOH). We find that this scheme is effective in increasing the model HO$_2$ levels by 24.2 % for terpene levels >80 pptv (Figure 6). Since we have used a very simple approach to test the impact of autoxidation in the model atmosphere, more studies are required towards a mechanistic development for incorporating these schemes viz. which way the H-shift will occur at which rate, which products will be formed, etc. The present exercise in implementing the autoxidation scheme is only meant to show its

10 importance, effectiveness and potential in atmospheric chemistry models.

3.5 HO$_x$ chemistry during CYPHEX: production and loss estimates

Using the optimal scenario from our model results, i.e. the one where all measured species are included in the model (case III, Figure 3), we can study different processes impacting HO$_x$ budgets. Since impact of terpene generated RO$_2$ species was maximum on day 210 (29 July), we will ignore any special features on this day for our subsequent discussions using the

15 model case III, the 'terpene case'. For CYPHEX, the major OH as well as HO$_x$ producing channel is the reaction of atmospheric water vapor with O^{1}D generated from the photolysis of O$_3$ (Figure 7). Peak daytime contributions of this channel towards OH production exceeded 45 % for most of the days, and about 60 % on days 205 and 208. The midday values coinciding with peak OH production on day 205 was marked by conspicuous influence of aged air masses originating over south-west Europe and considerably processed over the Mediterranean before reaching the site. The peak HO$_2$ values

20 on this day were about 11% lower than the average peak HO$_2$ values during the study period. The peak HO$_2$ values for J(O^{1}D)>2.5e^{-5} s^{-1} was 6.4 x 10^8 molec/cm^3 for the study period while this value was only 5.7 x 10^8 molec/cm^3 on day 205. While on average, the recycled OH via reactions of HO$_2$ with NO and O$_3$ (R6-R7) contributed 32 % to the total OH production, this value was about 6 % lower for days 205-206. It may also be noted that although O$_3$ was very low on both days 205 and 206, with predominant influence of aged marine air, the contribution from O^{1}D+H$_2$O to the total OH

25 production still exceeded 50 %. Due to lower HONO mixing ratios, the fractional contributions of HONO photolysis towards peak OH production during midday on days 207 and 208 were significantly low at about 2.5-3.4 %. On all other days, for which values are available, this channel contributed more than 5.9 % to peak OH production during noon time. The photolysis of HONO has the largest fractional contribution to the early morning OH production on day 211, reaching above 30 %. Overall during CYPHEX, the average daytime (JO^{1}D>0) contribution to OH production from O$_3$ photolysis and

30 subsequent reaction of O^{1}D with water vapor was about 37.2 %, the average daytime contribution from HONO photolysis was 12.0 %, while recycled OH from reaction of HO$_2$ with O$_3$ and NO account for 14.5 and 17.7 % of the total OH production, respectively. The four major OH producing channels (Figure 7) contribute 80-90 % of daytime OH production on most occasions, with 81.5 % on average.

The single major sink of OH during CYPHEX was CO, followed by CH$_4$, HCHO, C$_5$H$_8$, CH$_3$CHO and O$_3$, on average

35 accounting 20.3, 9.7, 7.6, 5.0, 4.8 and 4.0 % of OH losses respectively. During these days (205-206), the modelled OH loss (Figure 7) as well as the calculated OH reactivity (Figure 4) were lowest of the study period. It is likely that the air masses arriving to the site were already much processed, spending considerable time over the Atlantic and Mediterranean, leading to depleted OH reactivity. During this period of marine influence, the contribution of long-lived gases to the daytime OH loss increased by about 14% while the contribution of shorter lived gases like HCHO and CH$_3$CHO decreased by 36 % and 40 %

40 respectively. HCHO concentrations are observed to be lowest between days 205-206, when the marine influence was the highest. The average lifetime of HCHO for the study period is calculated to be 0.86 days, and its concentrations are higher whenever air masses are influenced by South-East Europe/ Black Sea region.

The major source of HO_2 during CYPHEX was the oxidation of CO by OH, contributing on average, 36.2 % of daytime HO_2 production values. On days 205, 206, when the site experienced aged oceanic air masses and CO concentrations were the lowest of the study period, yet the peak contribution of CO to daytime HO_2 production was about 40.4 %. This shows that the contribution from other HO_2 precursors like HCHO decreases much faster than CO because of their shorter lifetime as the air mass passes over the ocean, and isolated from their emission sources. The contributions of HCHO towards HO_2 production varied between 8-23 % with an average daytime contribution of 15.6 % and included both oxidation via OH and photolysis. The methoxy radical (CH_3O), formed during oxidation of CH_4 and CH_3O_2, was also a significant source of HO_2 with peak contributions reaching 23 % on some occasions and an average daytime contribution of 17.8 %. On average, the reactions of HO_2 with NO and O_3, recycling OH, contributed 23.3 and 18.2 % respectively towards daytime loss for HO_2. HO_2 losses by its self-reactions and reactions with CH_3O_2 reached peak daytime values of over 40 % and on average accounted for 29.5 % of daytime HO_2 losses. Among these, the major contribution was from the HO_2 self-reactions, with peak values of over 30 % during most days, and average values of 22.4 %. HO_2 losses due to recycling via NO and O_3 and the HO_2 losses via reactions with itself and CH_3O_2, are complementary during a diurnal cycle. The self-reactions gain in importance and peak around midday as the peroxy radical concentrations increase with increasing photochemistry, while recycling reactions dominate during periods with larger solar zenith angle. During CYPHEX, for small solar zenith angles with $J(O^1D)>2e^{-5}$ s^{-1}, the contribution of recycling and self-reactions to HO_2 loss was 36.2 and 32.7 % respectively. Overall, it is found that lowest HO_x production and losses occurred in the highly processed air masses influenced by the marine boundary layer, mostly over the Mediterranean Sea, but sometimes as far as the Atlantic ocean (days 205-206) with some influence from south-west Europe/northern Africa (Figure 7, panel 3).

The close proximity of Cyprus to several countries with different socio-economic conditions makes its air quality vulnerable to the increases or decreases of primary and secondary air pollutants in one of these countries in Europe, Asia and Africa. For example, increased NO_x emissions in one of the Southern European countries or high CO from forest fires in Ukraine can be quickly transported to Cyprus in a matter of hours to days and modulate the atmospheric processing over the region. Increased NO_x emissions can impact the O_3-NO_x-VOC chemistry by changing the HO_x cycling. Even though the study period was characterized by NO mostly<100 pptv, decreasing NO_x by 30 % still decreased OH levels by 14%, these impacts being higher in the early morning and late afternoon. On the other hand, increasing NO by 5 and 10 times caused 44 % and 70 % average enhancement in OH levels.

Because of its important role in O_3 production, NO_x emissions have been the focus of air quality investigations during preceding decades. Apart from their crucial role in O_3 production, NO_x levels also play a significant role in the self-cleaning capacity of the atmosphere due to their reactions with atmospheric HO_2 and RO_2. We test the impact of mainland Europe NO_x emissions on the self-cleaning capability of the climatically vulnerable Mediterranean atmosphere using the CYPHEX dataset. The recycling efficiency for OH (REf-OH) is defined as the ratio of OH produced from secondary sources via reactions of HO_2 with NO and O_3 (R6-R7) to the OH produced from primary and secondary sources. The primary sources of OH considered in our calculation include reaction of H_2O with O^1D produced from O_3 photolysis and the photolysis of HONO and H_2O_2.

While the present study is limited to NO <100 pptv, modelling results show that REf-OH increases with increase in NO levels (Figure 8). The REf-OH increases from 25 % at 10 pptv to about 40 % at around 20 pptv NO to about 70 % at 100 pptv NO (Figure 8). The relationship of REf-OH with NO indicates that at higher NO (not observed for the CYPHEX data), the REf-OH would increase further. To understand if REf-OH would reach runaway conditions or saturate at a particular value, we chose several points along the REf-OH-NO curve and for each of these points, we generated hypothetical input data set keeping all parameters constant but changing the NO_x levels from 0.2 to 3 ppbv, while maintaining the original NO/NO_2 ratio (Figure 8).

Figure 8 shows that in general the REf-OH increases to about 80 % at 400 pptv NO. After this, it decreases gradually, related to the reaction of NO_2 with OH. Concurrently, the loss of HO_2 due to self-reactions and reaction of HO_2 with CH_3O_2 becomes much weaker compared to the loss of HO_2 to NO with increasing NO levels. The ratio of HO_2 losses via the radical-radical interactions (i.e. the reactions of HO_2 with HO_2 and CH_3O_2) to the HO_2 losses via the recycling channel (i.e.
5 reactions of HO_2 with NO and O_3) decreases exponentially becoming less than 1 at 35 pptv NO and less than 0.5 at 70 pptv NO and 0.01 at 1 ppbv NO. The secondary OH production also shows a similar pattern with respect to REf-OH, peaking around 400 pptv for the different input data sets and decaying thereafter. The model generated OH peaks in this range but the HO_x concentrations start to drop much earlier, from around 70 pptv NO. At these low NO levels, HO_x loss by peroxide-peroxide reactions is comparable to the channels recycling HO_2 into OH, which can then be removed through reaction e.g.
10 with NO_2. However, the recycling efficiency is only about 60 % at 70 pptv NO. Budget analysis indicates that HO_x production drops with increasing NO levels for this test dataset constrained to specific NO_x levels. Overall, for the hydrocarbon levels observed during CYPHEX, the self-cleaning capacity of the atmosphere peaks at around 400 pptv NO, which at a NO/NO_2 ratio of 0.2 is equivalent to about 2.4 ppbv NO_x. Increasing NO_x emissions further would lead to decreased HO_x levels and the recycling efficiency is unlikely to increase further. On the other hand, decreasing NO levels
15 below a few hundred pptv of NO would also decrease the recycling efficiency for the same hydrocarbon levels indicating that small amount of NO_x help sustain the self-cleaning capacity of the atmosphere (Figure 8).

4. Conclusions

Atmospheric OH and HO_2 were measured as part of a comprehensive atmospheric chemistry field measurement campaign conducted in Cyprus in the summer of 2014 to study the major processes impacting atmospheric oxidation and air chemistry
20 in a relatively unpolluted coastal region, periodically influenced by long range transport of European emissions. A comprehensive suite of atmospheric chemistry measurements obtained during CYPHEX enabled a detailed investigation of atmospheric oxidation processes, using a photochemical box model, under low NO_x conditions. The box model (CAABA/MECCA with MOM chemistry) simulations for both OH and HO_2 agreed within 10% of the measured values except for cases when terpene (α- and β-pinene, limonene) mixing ratios exceeded 80 pptv. During these periods, inclusion
25 of terpenes which account for only 3.7 % of OH reactivity, causes the HO_2 model/measured ratio to be about 0.72 due to loss of HO_2 by reactions with terpene generated peroxy radicals. Comparison of alternative reaction pathways to reduce this unrealistic HO_2 loss showed that autoxidation can be an effective sink for the RO_2 species generated from terpene oxidation. However, low terpene and NO regimes, prevailing during CYPHEX, and the absence of limonene chemistry in the current model scheme, precluded a more rigorous analysis of the probable chemical pathways for RO_2 degradation in the
30 atmosphere. Further, there is evidence that the rate constant of CH_3O_2 with OH could be two times faster than used in the current models (Bossolasco et al., 2014). Applying this in general to other peroxides, the rate constants need to be revisited as they will have a non-negligible impact on the chemical composition of the atmosphere, especially in remote low NO_x environments where the peroxide lifetimes are relatively long. As already indicated in literature, there is large uncertainty in the rate coefficients of different RO_2 species with NO and HO_2 (King et al., 2001) which are scopes for future studies.

35 The radical budget analysis for CYPHEX showed that primary production of OH via photolysis of O_3 constituted the main OH source and peak daytime contributions from this channel exceeded 45 % for most of the days. The average daytime contribution from HONO photolysis was about 12 % but it exceeded 30 % in the early morning on a few occasions. The recycled OH from reaction of HO_2 with O_3 and NO accounted for 14.5 and 17.7 % of the total OH production, respectively. The maximum recycling efficiency was about 70 % for about 100 pptv NO. CO was not only the single major daytime sink
40 of OH, accounting for nearly one-fifth of OH loss during the study period, but also the single major HO_2 production source. Despite low NO_x regimes during CYPHEX, NO contributed more than 23 % of peak daytime loss for HO_2, reaching over 50 % on a few occasions. Lowest HO_x production and losses occurred in the highly processed air masses with low OH reactivity i.e. low precursor levels. These air masses were heavily influenced by the marine boundary layer, mostly by the Mediterranean Sea, but sometimes as far as the Atlantic Ocean (24-25 July, DOY 205-206) with some influence from south-

west Europe/northern Africa. Additionally, our results connote the need for deeper understanding of the reaction channels for organic peroxides in the atmosphere.

Data availability

Data are available on request from the CYPHEX archive at MPIC server. If desired, please send an email to
5 hartwig.harder@mpic.de.

Competing interests

The authors declare that they have no conflict of interest.

Acknowledgement

We acknowledge the contribution of the entire CYPHEX team, especially those members whose names are not listed as co-
10 authors, for the success of the CYPHEX campaign. We also acknowledge the administrative and logistic support provided by the Cyprus Institute and the officials at the army base at Inea. We sincerely acknowledge the technical support provided by the workshop and electronics department in the Max Planck Institute for Chemistry in preparation for the campaign. Further, technical help from Markus Rudolf, Korbinian Hens, Cheryl Ernest and Pippa Jones during preparation stage of the campaign is highly appreciated.

References

Atkinson, R., Baulch, D. L., Cox, R. A., Hampson, R. F., Kerr, J. A., Rossi, M. J., Troe, J., and Evaluation, I. S. G. K. D.: Evaluated kinetic and photochemical data for atmospheric chemistry, organic species: Supplement VII, *J Phys Chem Ref Data*, **28**, 191-393, Doi 10.1063/1.556048, 1999.

20 Berresheim, H., Plass-Dulmer, C., Elste, T., Mihalopoulos, N., and Rohrer, F.: OH in the coastal boundary layer of Crete during MINOS: Measurements and relationship with ozone photolysis, *Atmospheric Chemistry and Physics*, **3**, 639-649, 2003.

Bossolasco, A., Farago, E. P., Schoemaecker, C., and Fittschen, C.: Rate constant of the reaction between CH3O2 and OH radicals, *Chem Phys Lett*, **593**, 7-13, 10.1016/j.cplett.2013.12.052, 2014.

25 Boyd, A. A., Lesclaux, R., Jenkin, M. E., and Wallington, T. J.: A spectroscopic, kinetic, and product study of the (CH3)(2)C(OH)CH2O2 radical self-reaction and reaction with HO2, *J Phys Chem-Us*, **100**, 6594-6603, Doi 10.1021/jp953292c, 1996.

Brune, W. H., Stevens, P. S., and Mather, J. H.: Measuring Oh and Ho2 in the Troposphere by Laser-Induced Fluorescence at Low-Pressure, *J Atmos Sci*, **52**, 3328-3336, Doi 10.1175/1520-0469(1995)052<3328:Moahit>2.0.Co;2, 1995.

Calogirou, A., Larsen, B. R., and Kotzias, D.: Gas-phase terpene oxidation products: a review, *Atmos Environ*, **33**, 1423-1439, Doi 10.1016/S1352-2310(98)00277-5, 1999.

Carslaw, N., Creasey, D. J., Harrison, D., Heard, D. E., Hunter, M. C., Jacobs, P. J., Jenkin, M. E., Lee, J. D., Lewis, A. C., Pilling, M. J., Saunders, S. M., and Seakins, P. W.: OH and HO2 radical chemistry in a forested region of north-western Greece, *Atmos Environ*, **35**, 4725-4737, Doi 10.1016/S1352-2310(01)00089-9, 2001.

Crosley, D. R.: The Measurement of Oh and Ho2 in the Atmosphere, *J Atmos Sci*, **52**, 3299-3314, Doi 10.1175/1520-0469(1995)052<3299:Tmooah>2.0.Co;2, 1995.

Crounse, J. D., Nielsen, L. B., Jorgensen, S., Kjaergaard, H. G., and Wennberg, P. O.: Autoxidation of Organic Compounds in the Atmosphere, *J Phys Chem Lett*, **4**, 3513-3520, 10.1021/jz4019207, 2013.

Derstroff, B., Hüser, I., Bourtsoukidis, E., Crowley, J. N., Fischer, H., Gromov, S., Harder, H., Janssen, R. H. H., Kesselmeier, J., Lelieveld, J., Mallik, C., Martinez, M., Novelli, A., Parchatka, U., Phillips, G. J., Sander, R., Sauvage, C., Schuladen, J., Stönner, C., Tomsche, L., and Williams, J.: Volatile organic compounds (VOCs) in photochemically aged air from the eastern and western Mediterranean, *Atmos. Chem. Phys.*, **17**, 9547-9566, Doi 10.5194/acp-17-9547-2017, 2017.

Doche, C., Dufour, G., Foret, G., Eremenko, M., Cuesta, J., Beekmann, M., and Kalabokas, P.: Summertime tropospheric-ozone variability over the Mediterranean basin observed with IASI, *Atmospheric Chemistry and Physics*, **14**, 10589-10600, Doi 10.5194/acp-14-10589-2014, 2014.

Evans, M. J., Shallcross, D. E., Law, K. S., Wild, J. O. F., Simmonds, P. G., Spain, T. G., Berrisford, P., Methven, J., Lewis, A. C., McQuaid, J. B., Pilling, M. J., Bandy, B. J., Penkett, S. A., and Pyle, J. A.: Evaluation of a Lagrangian box model using field measurements from EASE (Eastern Atlantic Summer Experiment) 1996, *Atmos Environ*, **34**, 3843-3863, Doi 10.1016/S1352-2310(00)00184-9, 2000.

Fuchs, H., Bohn, B., Hofzumahaus, A., Holland, F., Lu, K. D., Nehr, S., Rohrer, F., and Wahner, A.: Detection of HO2 by laser-induced fluorescence: calibration and interferences from RO2 radicals, *Atmos Meas Tech*, **4**, 1209-1225, 10.5194/amt-4-1209-2011, 2011.

Gros, V., Williams, J., van Aardenne, J. A., Salisbury, G., Hofmann, R., Lawrence, M. G., von Kuhlmann, R., Lelieveld, J., Krol, M., Berresheim, H., Lobert, J. M., and Atlas, E.: Origin of anthropogenic hydrocarbons and halocarbons measured in the summertime european outflow (on Crete in 2001), *Atmospheric Chemistry and Physics*, **3**, 1223-1235, 2003.

Hard, T. M., Obrien, R. J., Chan, C. Y., and Mehrabzadeh, A. A.: Tropospheric Free-Radical Determination by Fage, *Environ Sci Technol*, **18**, 768-777, Doi 10.1021/es00128a009, 1984.

Heland, J., Ziereis, H., Schlager, H., de Reus, M., Traub, M., Lelieveld, J., Roelofs, G. J., Stock, P., and Roiger, A.: Aircraft measurements of nitrogen oxides, ozone, and carbon monoxide during MINOS 2001: distributions and correlation analyses, *Atmos. Chem. Phys. Discuss.*, **2003**, 1991-2026, Doi 10.5194/acpd-3-1991-2003, 2003.

Hens, K., Novelli, A., Martinez, M., Auld, J., Axinte, R., Bohn, B., Fischer, H., Keronen, P., Kubistin, D., Nolscher, A. C., Oswald, R., Paasonen, P., Petaja, T., Regelin, E., Sander, R., Sinha, V., Sipila, M., Taraborrelli, D., Ernest, C. T., Williams, J., Lelieveld, J., and Harder, H.: Observation and modelling of HOx radicals in a boreal forest, *Atmospheric Chemistry and Physics*, **14**, 8723-8747, Doi 10.5194/acp-14-8723-2014, 2014.

5   Hildebrandt, L., Kostenidou, E., Mihalopoulos, N., Worsnop, D. R., Donahue, N. M., and Pandis, S. N.: Formation of highly oxygenated organic aerosol in the atmosphere: Insights from the Finokalia Aerosol Measurement Experiments, *Geophys Res Lett*, **37**, Artn L23801, Doi 10.1029/2010gl045193, 2010.

Huser, I., Harder, H., Heil, A., and Kaiser, J. W.: Assumptions about footprint layer heights influence the quantification of emission sources: a case study for Cyprus, *Atmospheric Chemistry and Physics*, **17**, 10955-10967, Doi 10.5194/acp-17-
10   10955-2017, 2017.

Jenkin, M. E., Saunders, S. M., and Pilling, M. J.: The tropospheric degradation of volatile organic compounds: A protocol for mechanism development, *Atmos Environ*, **31**, 81-104, Doi 10.1016/S1352-2310(96)00105-7, 1997.

Kalabokas, P. D., Cammas, J. P., Thouret, V., Volz-Thomas, A., Boulanger, D., and Repapis, C. C.: Examination of the atmospheric conditions associated with high and low summer ozone levels in the lower troposphere over the eastern
15   Mediterranean, *Atmospheric Chemistry and Physics*, **13**, 10339-10352, Doi 10.5194/acp-13-10339-2013, 2013.

King, M. D., Canosa-Mas, C. E., and Wayne, R. P.: Gas-phase reactions between RO2 and NO, HO2 or CH3O2: correlations between rate constants and the SOMO energy of the peroxy (RO2) radical, *Atmos Environ*, **35**, 2081-2088, Doi 10.1016/S1352-2310(00)00501-X, 2001.

Kleanthous, S., Vrekoussis, M., Mihalopoulos, N., Kalabokas, P., and Lelieveld, J.: On the temporal and spatial variation of
20   ozone in Cyprus, *Sci Total Environ*, **476**, 677-687, Doi 10.1016/j.scitotenv.2013.12.101, 2014.

Knote, C., Tuccella, P., Curci, G., Emmons, L., Orlando, J. J., Madronich, S., Baro, R., Jimenez-Guerrero, P., Luecken, D., Hogrefe, C., Forkel, R., Werhahn, J., Hirtl, M., Perez, J. L., San Jose, R., Giordano, L., Brunner, D., Yahya, K., and Zhang, Y.: Influence of the choice of gas-phase mechanism on predictions of key gaseous pollutants during the AQMEII phase-2 intercomparison, *Atmos Environ*, **115**, 553-568, Doi 10.1016/j.atmosenv.2014.11.066, 2015.

25   Kormann, R., Fischer, H., de Reus, M., Lawrence, M., Bruhl, C., von Kuhlmann, R., Holzinger, R., Williams, J., Lelieveld, J., Warneke, C., de Gouw, J., Heland, J., Ziereis, H., and Schlager, H.: Formaldehyde over the eastern Mediterranean during MINOS: Comparison of airborne in-situ measurements with 3D-model results, *Atmospheric Chemistry and Physics*, **3**, 851-861, 2003.

Lee, J. D., Young, J. C., Read, K. A., Hamilton, J. F., Hopkins, J. R., Lewis, A. C., Bandy, B. J., Davey, J., Edwards, P.,
30   Ingham, T., Self, D. E., Smith, S. C., Pilling, M. J., and Heard, D. E.: Measurement and calculation of OH reactivity at a United Kingdom coastal site, *J Atmos Chem*, **64**, 53-76, Doi 10.1007/s10874-010-9171-0, 2009.

Lelieveld, J., and Dentener, F. J.: What controls tropospheric ozone?, *J Geophys Res-Atmos*, **105**, 3531-3551, Doi 10.1029/1999jd901011, 2000.

Lelieveld, J., Berresheim, H., Borrmann, S., Crutzen, P. J., Dentener, F. J., Fischer, H., Feichter, J., Flatau, P. J., Heland, J., Holzinger, R., Korrmann, R., Lawrence, M. G., Levin, Z., Markowicz, K. M., Mihalopoulos, N., Minikin, A., Ramanathan, V., de Reus, M., Roelofs, G. J., Scheeren, H. A., Sciare, J., Schlager, H., Schultz, M., Siegmund, P., Steil, B., Stephanou, E. G., Stier, P., Traub, M., Warneke, C., Williams, J., and Ziereis, H.: Global air pollution crossroads over the Mediterranean, *Science*, **298**, 794-799, Doi 10.1126/science.1075457, 2002.

Lelieveld, J., Dentener, F. J., Peters, W., and Krol, M. C.: On the role of hydroxyl radicals in the self-cleansing capacity of the troposphere, *Atmospheric Chemistry and Physics*, **4**, 2337-2344, 2004.

Lelieveld, J., Hadjinicolaou, P., Kostopoulou, E., Chenoweth, J., El Maayar, M., Giannakopoulos, C., Hannides, C., Lange, M. A., Tanarhte, M., Tyrlis, E., and Xoplaki, E.: Climate change and impacts in the Eastern Mediterranean and the Middle East, *Climatic Change*, **114**, 667-687, Doi 10.1007/s10584-012-0418-4, 2012.

Lelieveld, J., Evans, J. S., Fnais, M., Giannadaki, D., and Pozzer, A.: The contribution of outdoor air pollution sources to premature mortality on a global scale, *Nature*, **525**, 367-+, 10.1038/nature15371, 2015.

Levy, H.: Normal Atmosphere - Large Radical and Formaldehyde Concentrations Predicted, *Science*, **173**, 141-&, Doi 10.1126/science.173.3992.141, 1971.

Lewis, A. C., Hopkins, J. R., Carpenter, L. J., Stanton, J., Read, K. A., and Pilling, M. J.: Sources and sinks of acetone, methanol, and acetaldehyde in North Atlantic marine air, *Atmospheric Chemistry and Physics*, **5**, 1963-1974, 2005.

Li, J. S., Reiffs, A., Parchatka, U., and Fischer, H.: In Situ Measurements of Atmospheric Co and Its Correlation with Nox and O-3 at a Rural Mountain Site, *Metrol Meas Syst*, **22**, 25-38, 2015.

Librando, V., and Tringali, G.: Atmospheric fate of OH initiated oxidation of terpenes. Reaction mechanism of alpha-pinene degradation and secondary organic aerosol formation, *J Environ Manage*, **75**, 275-282, Doi 10.1016/j.jenvman.2005.01.001, 2005.

Mao, J., Ren, X., Brune, W. H., Olson, J. R., Crawford, J. H., Fried, A., Huey, L. G., Cohen, R. C., Heikes, B., Singh, H. B., Blake, D. R., Sachse, G. W., Diskin, G. S., Hall, S. R., and Shetter, R. E.: Airborne measurement of OH reactivity during INTEX-B, *Atmospheric Chemistry and Physics*, **9**, 163-173, Doi 10.5194/acp-9-163-2009, 2009.

Martinez, M., Harder, H., Kubistin, D., Rudolf, M., Bozem, H., Eerdekens, G., Fischer, H., Klupfel, T., Gurk, C., Konigstedt, R., Parchatka, U., Schiller, C. L., Stickler, A., Williams, J., and Lelieveld, J.: Hydroxyl radicals in the tropical troposphere over the Suriname rainforest: airborne measurements, *Atmospheric Chemistry and Physics*, **10**, 3759-3773, 2010.

Mauldin, R. L., Berndt, T., Sipila, M., Paasonen, P., Petaja, T., Kim, S., Kurten, T., Stratmann, F., Kerminen, V. M., and Kulmala, M.: A new atmospherically relevant oxidant of sulphur dioxide, *Nature*, **488**, 193-196, Doi 10.1038/nature11278, 2012.

Meusel, H., Kuhn, U., Reiffs, A., Mallik, C., Harder, H., Martinez, M., Schuladen, J., Bohn, B., Parchatka, U., Crowley, J. N., Fischer, H., Tomsche, L., Novelli, A., Hoffmann, T., Janssen, R. H. H., Hartogensis, O., Pikridas, M., Vrekoussis, M., Bourtsoukidis, E., Weber, B., Lelieveld, J., Williams, J., Poschl, U., Cheng, Y. F., and Su, H.: Daytime formation of nitrous

acid at a coastal remote site in Cyprus indicating a common ground source of atmospheric HONO and NO, *Atmospheric Chemistry and Physics*, **16**, 14475-14493, Doi 10.5194/acp-16-14475-2016, 2016.

Nguyen, T. B., Crounse, J. D., Teng, A. P., Clair, J. M. S., Paulot, F., Wolfe, G. M., and Wennberg, P. O.: Rapid deposition of oxidized biogenic compounds to a temperate forest, *P Natl Acad Sci USA*, **112**, E392-E401, Doi 10.1073/pnas.1418702112, 2015.

Novelli, A., Hens, K., Ernest, C. T., Kubistin, D., Regelin, E., Elste, T., Plass-Dulmer, C., Martinez, M., Lelieveld, J., and Harder, H.: Characterisation of an inlet pre-injector laser-induced fluorescence instrument for the measurement of atmospheric hydroxyl radicals, *Atmos Meas Tech*, **7**, 3413-3430, Doi 10.5194/amt-7-3413-2014, 2014a.

Novelli, A., Vereecken, L., Lelieveld, J., and Harder, H.: Direct observation of OH formation from stabilised Criegee intermediates, *Phys Chem Chem Phys*, **16**, 19941-19951, Doi 10.1039/c4cp02719a, 2014b.

Ren, X. R., Olson, J. R., Crawford, J. H., Brune, W. H., Mao, J. Q., Long, R. B., Chen, Z., Chen, G., Avery, M. A., Sachse, G. W., Barrick, J. D., Diskin, G. S., Huey, L. G., Fried, A., Cohen, R. C., Heikes, B., Wennberg, P. O., Singh, H. B., Blake, D. R., and Shetter, R. E.: HOx chemistry during INTEX-A 2004: Observation, model calculation, and comparison with previous studies, *J Geophys Res-Atmos*, **113**, Artn D05310, Doi 10.1029/2007jd009166, 2008.

Rohrer, F., Lu, K. D., Hofzumahaus, A., Bohn, B., Brauers, T., Chang, C. C., Fuchs, H., Haseler, R., Holland, F., Hu, M., Kita, K., Kondo, Y., Li, X., Lou, S. R., Oebel, A., Shao, M., Zeng, L. M., Zhu, T., Zhang, Y. H., and Wahner, A.: Maximum efficiency in the hydroxyl-radical-based self-cleansing of the troposphere, *Nat Geosci*, **7**, 559-563, Doi 10.1038/Ngeo2199, 2014.

Salisbury, G., Williams, J., Holzinger, R., Gros, V., Mihalopoulos, N., Vrekoussis, M., Sarda-Esteve, R., Berresheim, H., von Kuhlmann, R., Lawrence, M., and Lelieveld, J.: Ground-based PTR-MS measurements of reactive organic compounds during the MINOS campaign in Crete, July-August 2001, *Atmospheric Chemistry and Physics*, **3**, 925-940, 2003.

Sander, R., Baumgaertner, A., Gromov, S., Harder, H., Jockel, P., Kerkweg, A., Kubistin, D., Regelin, E., Riede, H., Sandu, A., Taraborrelli, D., Tost, H., and Xie, Z. Q.: The atmospheric chemistry box model CAABA/MECCA-3.0, *Geosci Model Dev*, **4**, 373-380, Doi 10.5194/gmd-4-373-2011, 2011.

Silva, R. A., West, J. J., Zhang, Y. Q., Anenberg, S. C., Lamarque, J. F., Shindell, D. T., Collins, W. J., Dalsoren, S., Faluvegi, G., Folberth, G., Horowitz, L. W., Nagashima, T., Naik, V., Rumbold, S., Skeie, R., Sudo, K., Takemura, T., Bergmann, D., Cameron-Smith, P., Cionni, I., Doherty, R. M., Eyring, V., Josse, B., MacKenzie, I. A., Plummer, D., Righi, M., Stevenson, D. S., Strode, S., Szopa, S., and Zeng, G.: Global premature mortality due to anthropogenic outdoor air pollution and the contribution of past climate change, *Environ Res Lett*, **8**, Unsp 034005, Doi 10.1088/1748-9326/8/3/034005, 2013.

Sinha, V., Williams, J., Diesch, J. M., Drewnick, F., Martinez, M., Harder, H., Regelin, E., Kubistin, D., Bozem, H., Hosaynali-Beygi, Z., Fischer, H., Andres-Hernandez, M. D., Kartal, D., Adame, J. A., and Lelieveld, J.: Constraints on instantaneous ozone production rates and regimes during DOMINO derived using in-situ OH reactivity measurements, *Atmospheric Chemistry and Physics*, **12**, 7269-7283, Doi 10.5194/acp-12-7269-2012, 2012.

Smith, S. C., Lee, J. D., Bloss, W. J., Johnson, G. P., Ingham, T., and Heard, D. E.: Concentrations of OH and HO2 radicals during NAMBLEX: measurements and steady state analysis, *Atmospheric Chemistry and Physics*, **6**, 1435-1453, 2006.

Sobanski, N., Tang, M. J., Thieser, J., Schuster, G., Pohler, D., Fischer, H., Song, W., Sauvage, C., Williams, J., Fachinger, J., Berkes, F., Hoor, P., Platt, U., Lelieveld, J., and Crowley, J. N.: Chemical and meteorological influences on the lifetime of

5 NO3 at a semi-rural mountain site during PARADE, *Atmospheric Chemistry and Physics*, **16**, 4867-4883, Doi 10.5194/acp-16-4867-2016, 2016.

Stockwell, W. R., Kirchner, F., Kuhn, M., and Seefeld, S.: A new mechanism for regional atmospheric chemistry modeling, *J Geophys Res-Atmos*, **102**, 25847-25879, Doi 10.1029/97jd00849, 1997.

Stohl, A., Forster, C., Frank, A., Seibert, P., and Wotawa, G.: Technical note: The Lagrangian particle dispersion model

10 FLEXPART version 6.2, *Atmospheric Chemistry and Physics*, **5**, 2461-2474, 2005.

Stone, D., Whalley, L. K., and Heard, D. E.: Tropospheric OH and HO2 radicals: field measurements and model comparisons, *Chem Soc Rev*, **41**, 6348-6404, Doi 10.1039/c2cs35140d, 2012.

Taraborrelli, D., Lawrence, M. G., Butler, T. M., Sander, R., and Lelieveld, J.: Mainz Isoprene Mechanism 2 (MIM2): an isoprene oxidation mechanism for regional and global atmospheric modelling, *Atmospheric Chemistry and Physics*, **9**, 2751-

15 2777, 2009.

Taraborrelli, D., Lawrence, M. G., Crowley, J. N., Dillon, T. J., Gromov, S., Gross, C. B. M., Vereecken, L., and Lelieveld, J.: Hydroxyl radical buffered by isoprene oxidation over tropical forests, *Nat Geosci*, **5**, 190-193, Doi 10.1038/Ngeo1405, 2012.

Thornton, J. A., Wooldridge, P. J., Cohen, R. C., Martinez, M., Harder, H., Brune, W. H., Williams, E. J., Roberts, J. M.,

20 Fehsenfeld, F. C., Hall, S. R., Shetter, R. E., Wert, B. P., and Fried, A.: Ozone production rates as a function of NOx abundances and HOx production rates in the Nashville urban plume, *J Geophys Res-Atmos*, **107**, Artn 4146, Doi 10.1029/2001jd000932, 2002.

Tyrlis, E., Tymvios, F. S., Giannakopoulos, C., and Lelieveld, J.: The role of blocking in the summer 2014 collapse of Etesians over the eastern Mediterranean, *J Geophys Res-Atmos*, **120**, 6777-6792, 10.1002/2015jd023543, 2015.

25 Wisthaler, A., Jensen, N. R., Winterhalter, R., Lindinger, W., and Hjorth, J.: Measurements of acetone and other gas phase product yields from the OH-initiated oxidation of terpenes by proton-transfer-reaction mass spectrometry (PTR-MS), *Atmos Environ*, **35**, 6181-6191, Doi 10.1016/S1352-2310(01)00385-5, 2001.

Yang, Y. D., Shao, M., Wang, X. M., Nolscher, A. C., Kessel, S., Guenther, A., and Williams, J.: Towards a quantitative understanding of total OH reactivity: A review, *Atmos Environ*, **134**, 147-161, Doi 10.1016/j.atmosenv.2016.03.010, 2016.

30 Zhang, X., Mcvay, R. C., Huang, D. D., Dalleska, N. F., Aumont, B., Flagan, R. C., and Seinfeld, J. H.: Formation and evolution of molecular products in alpha-pinene secondary organic aerosol, *P Natl Acad Sci USA*, **112**, 14168-14173, Doi 10.1073/pnas.1517742112, 2015.

Rickard, A. and Pascoe, S.: The Master Chemical Mechanism (MCM), 2009, http://mcm.leeds.ac.uk/MCMv3.3.1/categories/saunders-2003-4_6_1-gen-master.htt?rxnId=6916;

Sander, S. P., J. Abbatt, J. R. Barker, J. B. Burkholder, R. R. Friedl, D. M. Golden, R. E. Huie, C. E. Kolb, M. J. Kurylo, G. K. Moortgat, V. L. Orkin. and P. H. Wine: Chemical Kinetics and Photochemical Data for Use in Atmospheric Studies, Evaluation No. 17, *JPL Publication* **10-6**, Jet Propulsion Laboratory, Pasadena, 2011, http://jpldataeval.jpl.nasa.gov.

IUPAC: Task Group on Atmospheric Chemical Kinetic Data Evaluation, Ammann, M., Cox, R.A., Crowley, J.N., Jenkin,
5   M.E., Mellouki, A., Rossi, M. J., Troe, J. and Wallington, T. J., http://iupac.pole-ether.fr/index.html., 2015.

Taraborrelli, D., Perez, D.C., Sander, R., and Pozzer, A., Geophysical Research Abstracts, EGU General Assembly, 17, EGU2015-12026, 2015   (meetingorganizer.copernicus.org/EGU2015/EGU2015-12026.pdf)

Yarwood, G., S. Rao, M. Yocke, G. Whitten, Updates to the Carbon Bond Mechanism: CB05, Report to the U.S. Environmental Protection Agency, 2005 (http://www.camx.com/publ/pdfs/CB05_Final_Report_120805.pdf)

10 European Union emission inventory report 1990–2015 under the UNECE Convention on Long-range Transboundary Air Pollution (LRTAP), 2017, https://www.eea.europa.eu/publications/annual-eu-emissions-inventory-report; http://www.eea.europa.eu/data-and-maps/data/data-viewers/air-emissions-viewer-lrtap.

Table 1: Details of experiments conducted during CYPHEX (relevant to this study) *Total uncertainty for the lower humidity range (< ca. 25% relative humidity)

Species	Measurement Technique	Time Resolution	Precision	Limit of Detection	Total Uncertainty	Reference
Hydroxyl Radical	LIF-FAGE-IPI	4 min	$4.8e5$ molec/cm^3	$1e^6$ molec/cm^3	28.5% (2σ)	(Hens et al., 2014)
Hydroperoxyl Radical	LIF-FAGE	14 sec	0.4 pptv	0.8 pptv	36% (2σ)	(Martinez et al., 2010)
Ozone	UV Photometry	1 min		2 ppbv	5%	(Li et al., 2015) (Beygi, 2011)
Carbon monoxide	Room Temperature Quantum Caascade Laser spectrometer	1 sec		0.4 ppbv	14.4%	(Li et al., 2015)
Nitric Oxide Nitrogen Dioxide	Chemiluminescence	5 sec		5 pptv 20 pptv	20% 30%	(Li et al., 2015) (Beygi, 2011)
Nitrous Acid	Long Path Absorption Photometry	30 sec		4 pptv	10%	(Meusel et al., 2016)
Formaldehyde	Hantzsch reaction fluorescence	10 min		38 pptv	16%	(Kormann, 2003)
Hydrogen peroxide Organic peroxides	Enzymatic reaction	10 min		14.9 pptv	16% 20%	(Fischer, 2015)
Methyl hydroperoxide	High Performance Liquid Chromatography	12 min	3%	25 pptv	9%	Hafermann et al. (in prep)
SO₂	Chemical Ionization Mass Spectrometer	10 mins		50 pptv	30%	
C₂-C₄ (alkanes, alkenes)	GC-FID	60 min	<5%	1-8 pptv	10%	(Sobanski et al., 2016)

Methane	GC-FID	1 min	2%	20 ppbv	2%	This Study
Isoprene	GC-MS	45 min	3.3 %	1ppt	14.5%	(Derstroff et al., 2017)
α-pinene			4.9 %	1ppt	15%	
β-pinene			8.8%	2ppt	16.7%	
Limonene			4.2%	1ppt	14.7%	
	PTR-TOF-MS	1 min	1 σ	3σ	1 σ	(Derstroff et al., 2017)
Benzene			5.4% (at ~280 pptv)	14 pptv	14% (21%*)	
Toluene			4.9% (at ~ 280 pptv)	12 pptv	14% (20%*)	
Isoprene oxidation products			5.0% (at ~ 260 pptv)	14 pptv	11% (14%*)	
MEK			3.8% (at ~ 280 pptv)	16 pptv	11% (16%*)	
Methanol			2.5% (at ~2800pptv)	242 pptv	37% (41%*)	
Acetaldehyde			2.2% (at ~ 1300 pptv)	85 pptv	22% (27%*)	
Acetone			1.4% (at ~ 2500 pptv)	97 pptv	10% (17%*)	
Acetic Acid			9.2 % (at ~ 900 pptv)	264 pptv	51%	

Table 2. Deposition velocities of some important species considered in the model scheme

Species	Deposition Velocity (cm s⁻¹)
Peroxides	4
PAN	0.2
NO₃	4
HNO₃	4
PINAL	0.6
HCOOH	1
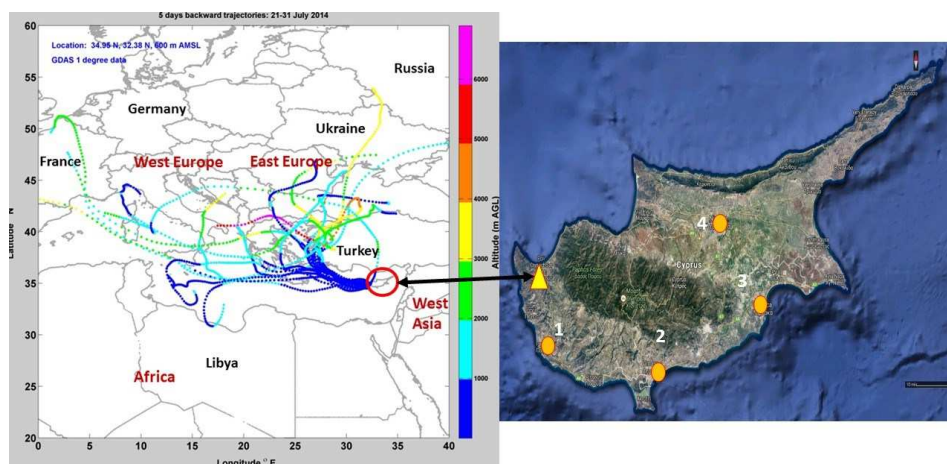
Figure 1. Left: Air masses during CYPHEX; Right: Map of Cyprus. Measurement site (yellow triangle), cities (circles, 1.Paphos, 2. Limassol 3. Larnaca 4. Nicosia)
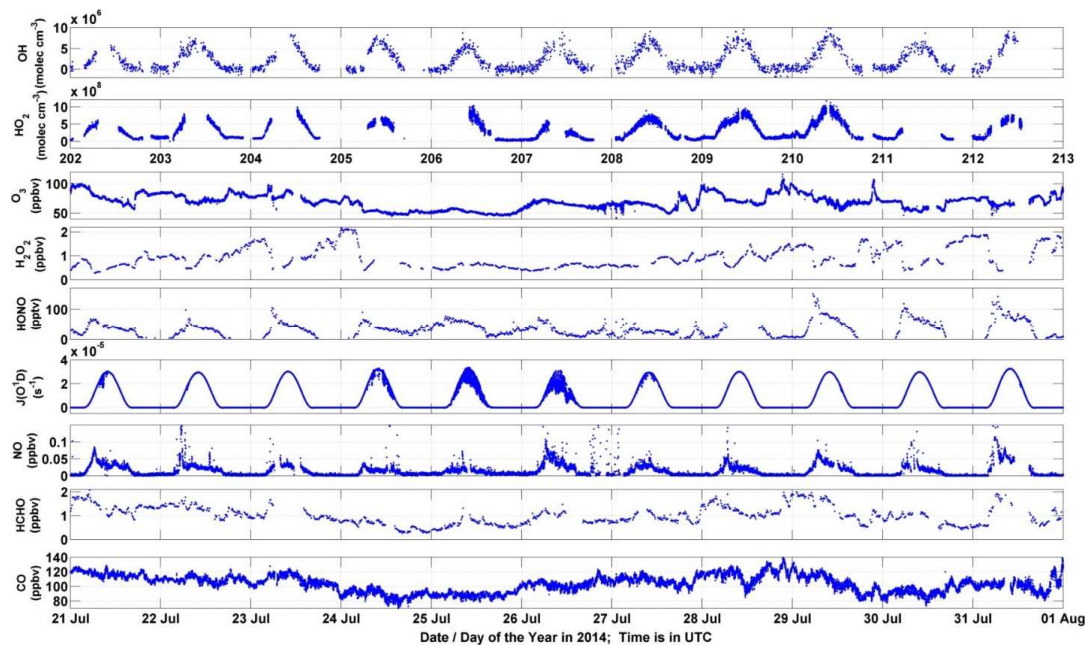
Figure 2. Measurements of OH, HO₂ along with selected chemical and radiation parameters relevant to HOₓ chemistry during the CYPHEX campaign. Time is in UTC. Local time in Cyprus during summer is UTC+3
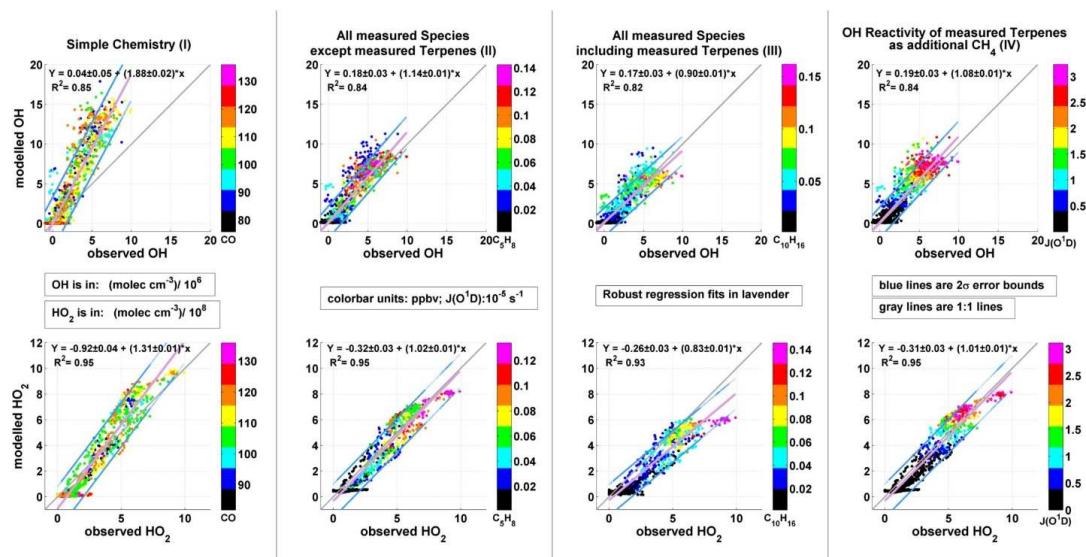
5 **Figure 3. LIF-FAGE measurements of OH (top panel) and HO₂ (bottom panel) vs model simulations with CAABA/MECCA. From left to right: model simulations using simple chemistry without NMHCs (case I), simulations including anthropogenic and biogenic hydrocarbons except terpenes (case II), after adding terpenes(case III) and after initializing with zero terpenes but with CH₄ increased to account for the additional measured terpene reactivity (case IV)**
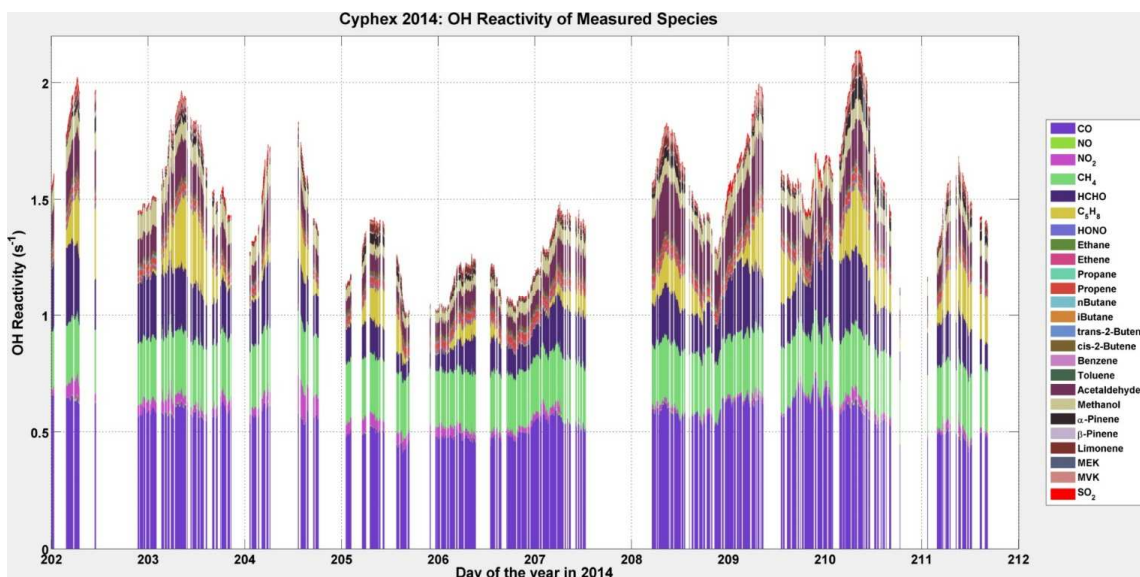
Figure 4. Calculated OH reactivity of various chemical species measured during CYPHEX
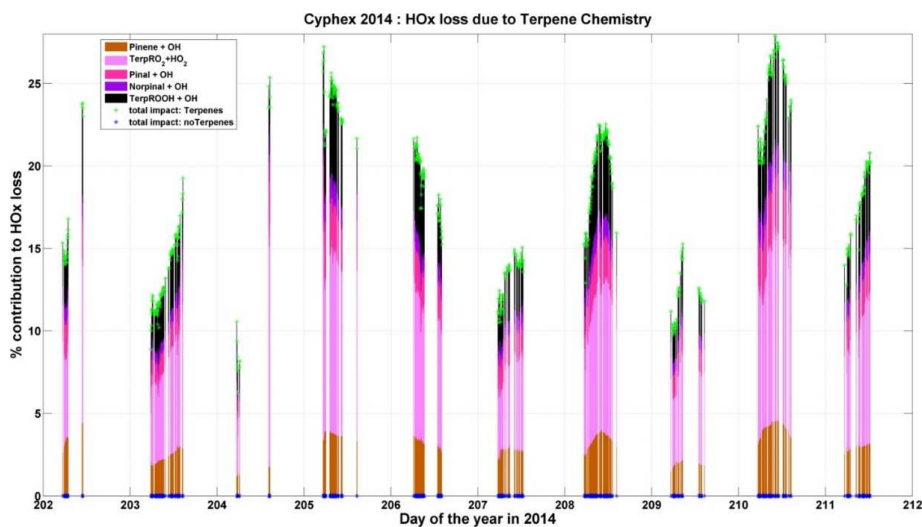
Figure 5. Contribution of different terpene related reactions to the total HO$_x$ loss. Additional peroxy radicals are produced in the model by terpenes rather than organics e.g. isoprene degradation. Pinene includes α-pinene and β-pinene. TerpRO2 include only

$C_8H_{13}O_3$ (C85O2), $C_8H_{13}O_4$ (C86O2), $C_9H_{15}O_3$ (C96O2), $C_9H_{15}O_4$ (C97O2), $C_9H_{15}O_5$ (C98O2), $C_{10}H_{15}O_5$ (C106O2), $C_5H_7O_4$ (C511O2), $C_6H_9O_5$ (C614O2), $C_{10}H_{15}O_4$ (PinalO2) and $C_{10}H_{17}O_3$ (BPinaO2). TerpROOH include only $C_{10}H_{16}O_4$ (PinalOOH), $C_8H_{14}O_3$ (C85OOH), $C_8H_{14}O_4$ (C86OOH), $C_9H_{16}O_4$ (C97OOH), $C_9H_{16}O_5$ (C98OOH), $C_{10}H_{16}O_5$ (C106OOH) and $C_5H_8O_4$ (C511OOH). The names in brackets are MCM nomenclature. Only those species are selected whose contribution is at least 0.25 %
5   to the HO_x sink
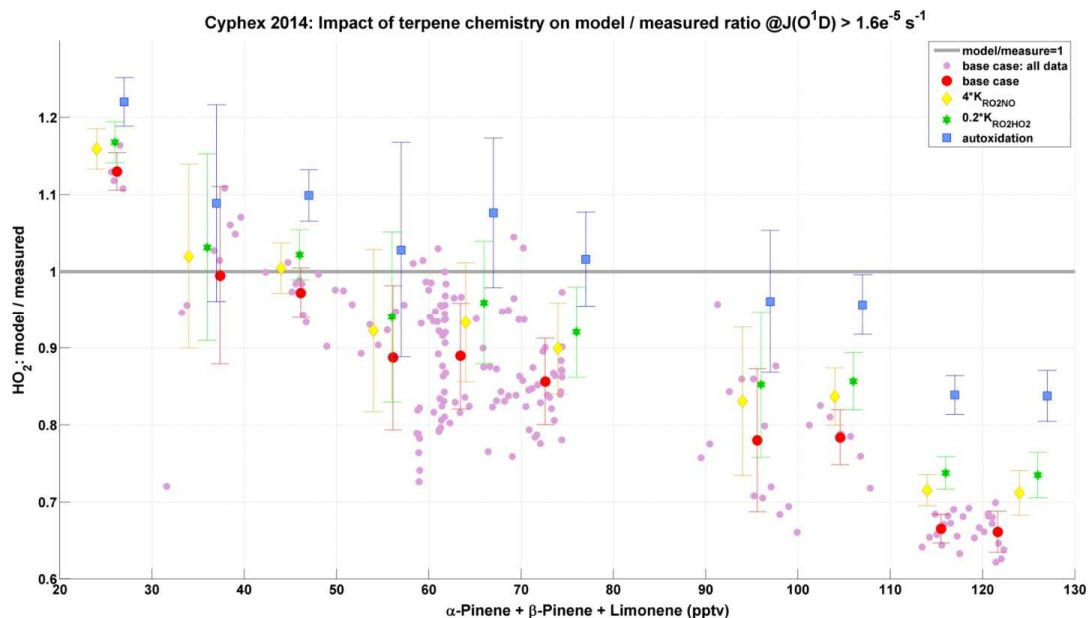
Figure 6. HO_2 predictions using different chemical schemes which were employed to investigate the impact of peroxy radicals as
10   HO_2 sink. The x-axis shows the sum of measured α-pinene, β-pinene and limonene. The base case is the model simulation using
measured species; $4*K_{RO2NO}$ is a simulation where the rates of selected terpene-related RO_2 species with NO are increased by a
factor of 4; $0.2*K_{RO2HO2}$ is a simulation where the rates of these RO_2 species with HO_2 are reduced by a factor of 0.2; the
autoxidation simulation includes an autoxidation scheme rapidly converting selected RO_2 species into ROOH. The mean and
sigma are calculated for 100 pptv bins along the x-axis
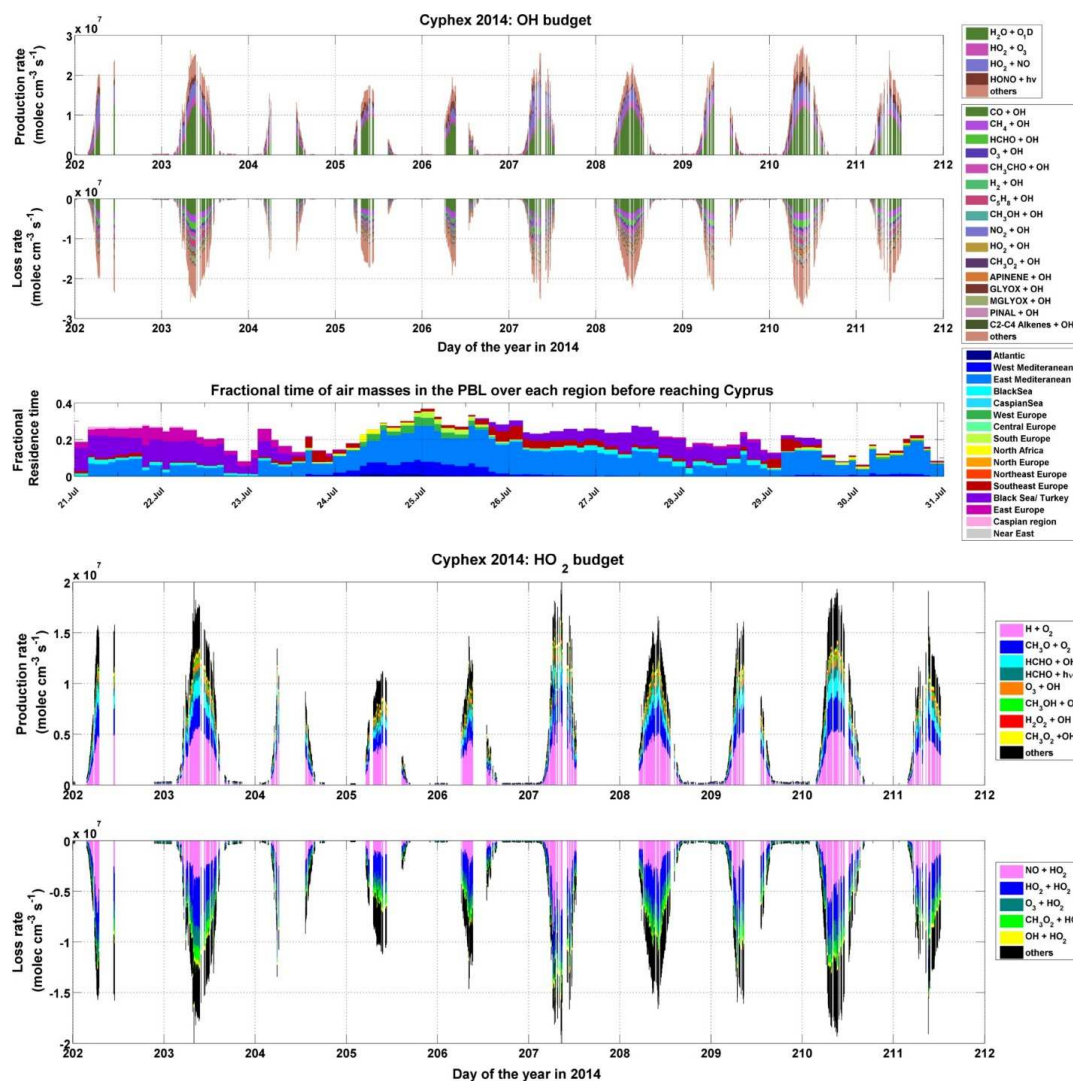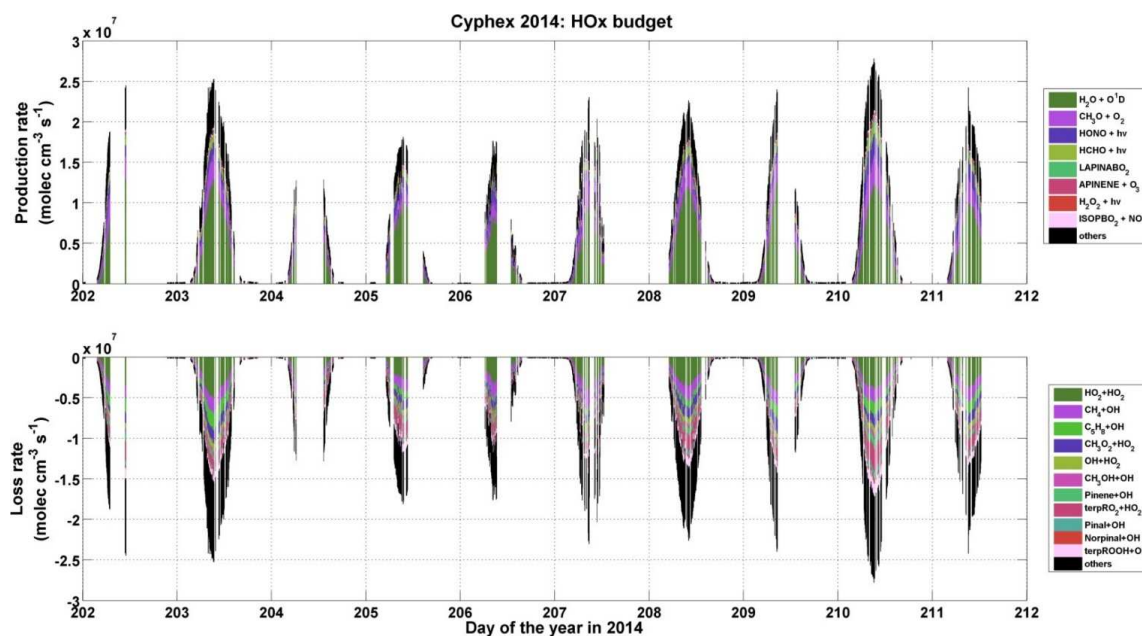
Figure 7. a. Budget analysis for OH during CYPHEX. The HO$_x$ budget is significantly impacted by the changes in air mass source regions. Flexpart evaluation of the contribution of different source regions within the planetary boundary layer to the air mass origin at the measurement site in Cyprus is shown in Panel 3. The air mass source regions are shown in a separate colour map (supplementary Figure 1). **b.** Budget analysis for HO$_2$, **c.** Budget analysis for HO$_x$, during CYPHEX. The descriptions for Pinene, terpRO$_2$ and terpROOH is same as in Figure 5
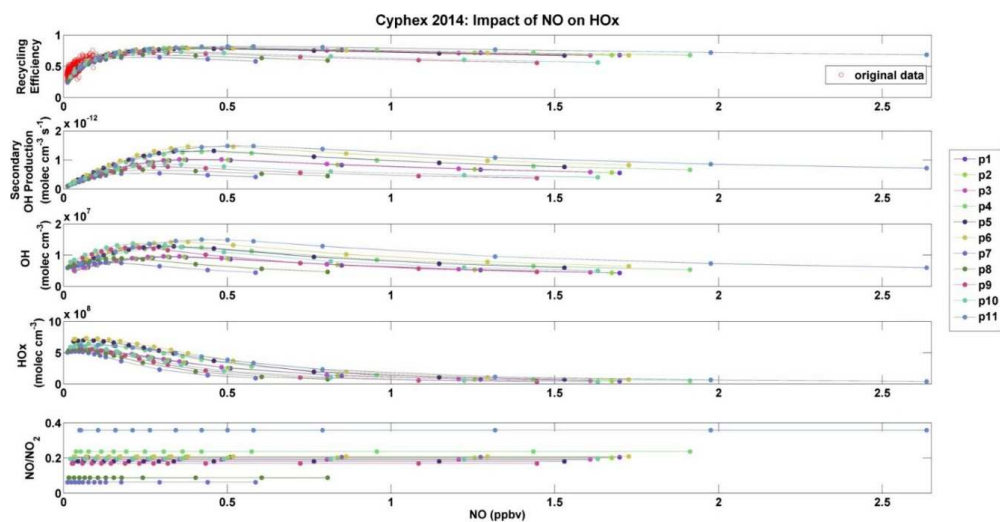
Figure 8. Sensitivity of recycling efficiency, secondary OH production, OH and HO$_x$ to changes in NO$_x$ levels. P1-P11 are different starting points derived from the original dataset, for which NO$_x$ is ramped up to 3 ppbv, while maintaining the original NO-NO$_2$

5   **ratio**